# Pelagic ecosystem responses to changes in seawater conditions during the Middle Pleistocene Transition in the Eastern Mediterranean

Konstantina Agiadi[1,2], Iuliana Vasiliev[3], Antoine Vite[4], Stergios Zarkogiannis[5], Alba Fuster-Alonso[2], Jorge Mestre-Tomás[2], Efterpi Koskeridou[6], Frédéric Quillévéré[4]

[1] Department of Geology, University of Vienna, Josef-Holaubek-Platz 2, UZA II, 1090, Vienna, Austria
[2] Renewable Marine Resources Department, Institute of Marine Sciences (ICM-CSIC), Passeig Marítim de la Barceloneta, 37-49, 08003 Barcelona, Spain
[3] Senckenberg Biodiversity Research Center (SbiK-F), Frankfurt am Main, Germany
[4] Université Claude Bernard Lyon 1, ENS de Lyon, CNRS, UMR 5276 LGL-TPE, F-69622 Villeurbanne, France
[5] University of Oxford, UK
[6] National and Kapodistrian University of Athens, Panepistimiopolis 15784, Athens, Greece

*Correspondence to*: Konstantina Agiadi (konstantina.agiadi@univie.ac.at)

**Abstract.** We present a multiproxy, ecosystem-level assessment of paleoenvironmental change and its impacts on marine organisms in the Eastern Mediterranean during the Middle Pleistocene Transition, between 923 and 756 kyr B.P. (marine isotope stages MIS 23–18). This study combines analyses of organic biomarkers; organic matter content; carbon and oxygen stable isotopes on bulk sediment, surface-dwelling, deep-dwelling planktonic and benthic foraminifera, ostracods and fish otoliths; as well as foraminiferal, ostracod and sponge abundance estimates, with a statistical assessment of paleoenvironmental regime shifts and estimation of fish distribution depths in the past. Our results show that temperature and productivity played the most important role in driving ecosystem changes in the study area at different times: temperature was the primary driver during MIS 21 interglacial, whereas productivity became a dominant factor in MIS 19 interglacial. In addition, the responses of organisms throughout the water column varied. Both interglacials yielded relatively higher plankton and benthos biomasses. However, for fishes, the responses differed. The abrupt global warming that occurred in early MIS 21, which was also captured by our record, probably led to a reduction in diel vertical migration by mesopelagic fishes and consequently to the efficiency of the biological carbon pump. In contrast, increased productivity across trophic levels is attested for MIS 19 that subsequently dropped in MIS 18, affecting foraminifera, ostracod and sponge biomasses, but not inhibiting fish diel vertical migration. Therefore, we conclude that carbon sequestration during MIS 19 was likely enhanced.

## 1 Introduction

The Middle Pleistocene Transition (MPT; 1.25–0.7 Ma) was an important period in recent climate evolution, marking the shift from the Pliocene symmetrical 41-ky to the modern 100-ky frequency, higher-amplitude, asymmetrical climate cycles

(Head and Gibbard, 2015). This shift was associated with the expansion of the Northern Hemisphere ice sheets (Ao et al., 2023; Berends et al., 2021; Clark et al., 2006; Elderfield et al., 2012) triggered by Antarctic ice-sheet growth (An et al., 2024) and led to major changes in the marine (Agiadi et al., 2011) and terrestrial biota (Cirilli et al., 2023), including a severe demographic crisis in human populations (Hu et al., 2023; Margari et al., 2023).

The conditions in the Mediterranean have been the topic of numerous studies because it was a hotspot of ancient human population change associated with the climate changes in the MPT (Margari et al., 2023). Sea surface temperature (SST) and primary productivity changes have been reconstructed with high temporal resolution in the Western and Central Mediterranean (Marino et al., 2020, 2022; Martínez-Dios et al., 2021; Nomade et al., 2019; Quivelli et al., 2021) and the southwestern Iberian margin (Girone et al., 2023; Rodrigues et al., 2017; Sánchez Goñi et al., 2023), providing up to millennial-scale paleoclimate reconstructions with even records of short-term extreme cooling events attributed to the reduction of the Atlantic Meridional Overturning Circulation. Very few studies have been conducted in the Eastern Mediterranean however (Eichner et al., 2024; Incarbona et al., 2022; Quillévéré et al., 2016, 2019). Particularly, a gap in knowledge remains regarding seawater conditions (i.e., temperature, thermal gradient, and salinity) and productivity in the Eastern Mediterranean during the MPT. The Eastern Mediterranean is currently affected by particularly much drier and ~4 °C warmer climatic conditions than the Western (Minnett et al., 2019). In addition, the riverine influx counterbalances, only up to a point, the negative water budget of the region promoted by extreme evaporation, and therefore much saltier sea surface conditions (> 39) prevail there than in the Western Mediterranean (~36.5). Such warmer and saltier conditions were last observed in the area in the Late Miocene (Besiou et al., 2024; Kontakiotis et al., 2022; Vasiliev et al., 2019) and it becomes intuitive that seawater conditions during the MPT may have also been very different from those in the Western Mediterranean.

Climate change affects the size and metabolism of marine organisms (Daufresne et al., 2009; Ohlberger, 2013), and consequently marine ecosystem structure and function (Hildrew et al., 2007). Although some aspects of the response of marine organisms to the paleoclimatic changes that occurred in the Mediterranean during the MPT have been studied so far, such as the composition of the calcareous nannoplankton (Marino et al., 2008, 2020), planktonic foraminifera (Quillévéré et al., 2019; Quivelli et al., 2021), and fish communities (Agiadi et al., 2011, 2018; Girone and Varola, 2001), as well as the body size of bivalves (Porz et al., 2024) and fishes (Agiadi et al., 2023), many questions remain about secondary production by zooplankton and zoobenthos, and the metabolic response of higher-trophic–level organisms.

Foraminifera are very sensitive to parameters of ambient seawater, such as food supply, light intensity, and sea temperature, which control community composition and pelagic biomass production (Gooday and Jorissen, 2012; Schiebel et al., 2018). In the case of the MPT, no consistent global patterns have been found, and productivity changes have been related mostly to regional changes in nutrient supply through variations in the hydrographic regime (Diester-Haass et al., 2018). With the production of their calcareous shells, both planktonic and benthic foraminifera actively contribute to the biological carbon pump (Grigoratou et al., 2022; Schiebel, 2002). However, quantifying their contribution to carbon export in the geological past has been hampered by the lack of estimates of their biomass. Although foraminifera are a very powerful tool for

paleoceanographic and paleoclimatic studies, these studies have almost exclusively been based on the assemblage composition, species abundance data or biogeochemical proxies, whereas very little is known about the fluctuations in foraminifera biomass in response to changes in environmental parameters. Planktonic foraminifera biomass is mainly controlled by temperature during the early stage of their development, but food availability becomes more important for adults (Grigoratou et al., 2019), whereas benthic foraminifera biomass is tightly linked to organic matter fluxes and oxygenation (Milker et al., 2019).

Ostracods are very sensitive to changes in the oxygen content of seawater (Huang et al., 2019), and paleoclimatic changes associated with the MPT severely affected the ostracod fauna composition and abundance in many areas worldwide (DeNinno et al., 2015; Huang et al., 2019) including the Mediterranean (Rossi et al., 2018).

Sponges are very attuned to seawater depth, pH, temperature, and oxygenation, making their assemblages and abundance very good indicators of paleoenvironmental conditions (Łukowiak, 2020). Sponge spicules in the sediment, reflecting biogenic silica accumulation over the MPT, have been used as a proxy of sea bottom conditions, reflecting cool, oxygen-rich water masses (Alvarez et al., 2017; Auer et al., 2021).

Fish respond swiftly to unfavorable environmental conditions by adjusting their geographic and depth distribution range (Perry et al., 2005), but changes in temperature, salinity, oxygenation and the availability of food eventually lead to eco-evolutionary shifts in their growth and mortality rates, size at maturity, and life-history patterns (Gallo and Levin, 2016; Lindmark et al., 2022; Rountrey et al., 2014). The MPT has already been shown to have affected the distribution and body size of fishes (Agiadi et al., 2018, 2023).

Mesopelagic fish of the family Myctophidae link trophic levels and play an essential role in the biological carbon pump through their diel vertical migration (Pinti et al., 2023). Diel vertical migration (DVM) is the daily movement of several marine organisms, including the mesopelagic fishes of the family Myctophidae, between the twilight (day-time) and the euphotic (night-time) zones (Brierley, 2014). Because these fishes feed at the surface and excrete and respire carbon at depth, their DVM leads to a net drawdown of carbon from the surface waters. According to some estimates, DVM contributes approximately 20% of the biological carbon pump in modern oceans, with more than 1 PgC/y being actively transported below the euphotic zone by all migrating organisms (Aumont et al., 2018). Compared with any other process of the biological carbon pump, carbon is directly injected deeper through the DVM (Aumont et al., 2018). As a result, the contribution of DVM to carbon sequestration accounts for to more than 50% of the global total, and mesopelagic fishes contribute half of this total (Aksnes et al., 2023; Pinti et al., 2023). The capacity of myctophids to perform DVM varies by species and is affected by seawater conditions, as are food availability and type (Olivar et al., 2018). Nothing is known about these regular movements of fishes in the geological past.

In this study, we investigate the responses of the pelagic ecosystem to changes in sea surface temperature, salinity, and primary productivity and relate these responses to the contemporaneous important climate changes that occurred during the MPT, between 923 and 756 kyr B.P., largely overlapping with MIS 23–MIS 18. We quantify changes in sea surface temperature (SST), sea surface salinity (SSS), and productivity. We use the findings to further tie the events to the observed

changes in important groups of pelagic life forms, namely planktonic foraminifera and ostracods (zooplankton), benthic foraminifera and sponges (benthos), and fishes (nekton). Using the isotopic compositions of foraminifera shells and fish otoliths, we infer the thermohaline gradient, detect shifts in the depth distribution and diel vertical migration patterns of myctophids, and derive changes in fish metabolism.

## 2 Material and Methods

### 2.1 Study area, sampling and chronostratigraphic background

The material used in this study originates from the Lindos Bay Formation exposed at Lardos, northeastern Rhodes, Greece (Fig. 1a). On the island of Rhodes, the Mesozoic–Paleogene limestone substratum is overlain by marine siliciclastic–carbonate Pleistocene deposits. Since the Pliocene, the compressive regime of this area of the Hellenic forearc and the concomitant opening of the > 4000 m deep Rhodes Basin have triggered rapid vertical tectonic motions resulting in the deposition and uplift of Pleistocene marine sediments that are now exposed along the eastern coast of the island (Cornée et al., 2006, 2019; Van Hinsbergen et al., 2007). The Early–Middle Pleistocene hemipelagic sediments of the Lindos Bay Formation sampled for this study were deposited at bathyal depths during the maximum flooding of this tectonically driven transgression–regression cycle (Cornée et al., 2019; Milker et al., 2017; Quillévéré et al., 2019). This occurrence of Pleistocene deep-water sediments accessible on land is unique for the Eastern Mediterranean, providing a valuable reference point for studying the Early–Middle Pleistocene marine faunas of the region (Quillévéré et al., 2016).

The studied section (36°05'19.5"N 28°00'35.9"E) is located at the northern flank of a hill positioned ~900 m southwest of the village of Lardos. The total section comprises 30 meters of marine marls and silts. In this work, we focus on the 2.4 m lowest marls of the section already studied by Titschack et al. (2013), and we dug a pit beneath them to extend the MPT record to a total thickness of 3.1 m. Thirty-two samples were obtained every 10 cm after the outcrop surface was refreshed.

A chronostratigraphic framework has been previously established for this section on the basis of nannoplankton and foraminiferal biostratigraphic analyses, oxygen isotopic compositions of surface-dwelling planktonic foraminifera, and $U^{234}/U^{238}$ dating of deep-water *Desmophyllum pertusum* coral fragments collected in an ~25–cm-thick horizon at ~2.3 m section height, which yielded mean ages of 755.2 ± 15.5 and 756.0 ± 17.5 kyr (Titschack et al., 2013). Taken together, these data revealed that the lowermost part of the Lardos section recovers the Early–Middle Pleistocene boundary (774 kyr) and the MPT interval between Marine Isotope Stage (MIS) 22 (*partim*) and MIS 18. By digging a pit at the base of the section, we extend the record down to MIS 23. In addition, by comparing new local $\delta^{18}O$ compositions of monospecific samples of benthic and planktonic foraminifera (see subsection 2.5) to those occurring in the global ocean (Lisiecki and Raymo, 2005) and Mediterranean reference records (Konijnendijk et al., 2015; Wang et al., 2010), we aim to refine the location in the section of climatic cycle terminations within the MIS 23–18 interval.

## 2.2 Paleodepth estimates

The 32 sediment samples were dried in an oven, weighed and placed in water and Calgon for five hours on a shaker table. The samples were subsequently sieved through a 63-µm mesh sieve and dried in an oven at 60 °C, after which the residues were weighed. The depositional depths through the 3.1 m sedimentary unit were assessed by counting the number of planktonic foraminifera *P* relative to the total number of planktonic and benthic foraminifera *(P+B)* (up to 300 planktonic foraminifera) in representative splits of the >125 µm size fraction of the 32 collected samples. Indeed, the planktonic/benthic ratio *%P(P+B)* typically increases with water depth or distance from shorelines (Gibson, 1989). We estimated the paleodepth *D* via the transfer function developed by van der Zwaan et al. (1990) (Eq. 1):

$$D = e^{3.58718} + 0.03534 \times \%P/(P+B) \quad (1)$$

Several limiting factors play a significant role in controlling benthic and/or planktonic foraminifera depth distribution, notably the sensitivity of benthic foraminifera assemblages to changes in the oxygen levels of the bottom waters (Jorissen et al., 1995), thus leading to potentially biased paleodepth estimates. We consequently followed the methodology proposed by van der Zwaan et al. (1990), discarding from the counts the infaunal benthic genera *Uvigerina*, *Bolivina*, *Bulimina*, *Globobulimina* and *Fursenkoina* as characteristic of organic-rich and oxygen-deficient environments.

## 2.3 Oxygen and carbon isotope analyses

The stable oxygen ($\delta^{18}$O) and carbon ($\delta^{13}$C) isotopic compositions were first measured on ground bulk sedimentary rock samples of the 32 collected horizons. The $\delta^{18}$O and $\delta^{13}$C values were also measured on shells of benthic (*Uvigerina peregrina*) and planktonic foraminifera (*Globigerinoides ruber*, *Globoconella inflata*), planktonic ostracods (*Bairdopilata* spp.), and fish otoliths (*Hygophum benoiti*, *Ceratoscopelus maderensis*).

*Uvigerina peregrina*, which occurs continuously in the section, is a shallow infaunal benthic species whose $\delta^{18}$O and $\delta^{13}$C values mirror the physical conditions and compositions of ambient bottom waters at the time of calcification. Time-series analysis of $\delta^{18}$O values measured in *Uvigerina peregrina* constitutes a powerful practical tool for global–scale correlation (Elderfield et al., 2012). *Globigerinoides ruber*, which also occurs continuously in the section, is a symbiont bearing planktonic species that preferably calcifies in the oligotrophic upper-most part of the water column (Schiebel and Hemleben, 2017). *Globoconella inflata* occurs in 29 out of the 32 collected samples and is an algal symbiont-barren planktonic species that calcifies mainly at intermediate depths of the photic zone in stratified water masses or in nutrient-rich surface waters (Schiebel and Hemleben, 2017). All $\delta^{18}$O and $\delta^{13}$C measurements on foraminifera were performed on shells handpicked from the 250–355 µm size fraction. About 10 to 15, 20 to 25 and 15 to 20 shells of *U. peregrina*, *G. ruber* and *G. inflata*, respectively, were analyzed per sample to supply sufficient calcium carbonate and to limit the effect of individual variation on the isotopic values (Agiadi et al., 2024b). The foraminifera shells analyzed were free of carbonate infilling or visible dissolution features. The samples were ultrasonically cleaned in distilled water, and weighed prior to isotopic analyses.

We also measured the $\delta^{18}O$ and $\delta^{13}C$ isotopic compositions of *Bairdopilata* spp. ostracods (2 to 4 valves per sample), which were found in 15 out of the 32 collected samples, and those of otoliths of the mesopelagic fish species *Hygophum benoiti* (9 samples) and *Ceratoscopelus maderensis* (8 samples) (Agiadi et al., 2024b).

Otoliths are aragonitic, incremental hard parts of the inner ear of teleost fishes, which are metabolically inert (Campana, 1999). Their $\delta^{18}O$ values depend on temperature and the $\delta^{18}O$ values of ambient water, and they are not affected by fish somatic or otolith growth (Kalish, 1991a). In a paleoceanographic setting, it has also been shown that the $\delta^{18}O$ values of otoliths of epipelagic fish closely follow those of planktonic foraminifera, whereas the $\delta^{18}O$ values of benthic fish otoliths fall within the range of those measured in benthic foraminifera from the same sediment samples (Agiadi et al., 2024a). The $\delta^{13}C$ of otoliths reflects the $\delta^{13}C$ of the fish diet and that of the dissolved inorganic carbon, and it is therefore a proxy of the fish metabolic rate (Chung et al., 2019a, b; Kalish, 1991a; Martino et al., 2020; Smoliński et al., 2021; Solomon et al., 2006; Trueman et al., 2016, 2023). In fossil fish otoliths, $\delta^{13}C$ has already been successfully used as a metabolic proxy (Agiadi et al., 2024a; Wurster and Patterson, 2003).

The two fish species were selected because they are among the most common myctophid species still living today in the Mediterranean (Mytilineou et al., 2005; Olivar et al., 2012), with very broad geographic distributions (Eduardo et al., 2021; Olivar et al., 2017; Zelck and Klein, 1995), and they are the most abundant in the Pleistocene fossil record (Agiadi et al., 2010, 2011, 2018, 2023; Girone et al., 2006).

All the ostracods and otoliths were sonicated in MeOH for about 10 s to remove adhering clay particles, rinsed at least five times in ultraclean water and dried under a clean-air flow. Randomly selected specimens were observed under a stereoscope to confirm their good preservation state (Agiadi et al., 2022; Antonarakou et al., 2019; Dufour et al., 2000). For the otoliths, a single specimen per sample was crushed, homogenized and analyzed.

The bulk samples were dried and drilled with a manual electric drill at the SBiK-F laboratory after being tested with HCl 10% for carbonate presence. The obtained powder was weighed and calibrated against standard reference materials (Carrara marble, NBS 18 and Merck). The $\delta^{18}O$ and $\delta^{13}C$ ratios were analyzed at Goethe University, Germany, using a Thermo Scientific MAT 253 mass spectrometer coupled to a GasBench II type with continuous flow using the calibration of Spötl and Vennemann (2003). Isotopic values were calculated against a $CO_2$ reference gas with a precision of 0.008‰ for $\delta^{18}O$ and 0.06‰ for $\delta^{13}C$. All values are presented with respect to Vienna Pee Dee Belemnite (VPDB).

The foraminifera, ostracod, and otolith $\delta^{18}O$ and $\delta^{13}C$ measurements were performed using an Elemental Multiprep system in line with a dual Inlet IsoPrime™ Isotope Ratio Mass Spectrometer (IRMS) at the Université Claude Bernard Lyon 1, France. The principle of the fully automated device is to react the calcium carbonates of foraminifera, ostracods or otoliths with anhydrous phosphoric acid at 90 °C to generate $CO_2$, which is then analyzed with IRMS. Isotopic compositions were quoted in the standard $\delta$ notation in per mil (‰) relative to V-PDB for both $^{18}O/^{16}O$ and $^{13}C/^{12}C$. All sample measurements were adjusted to the international reference NBS18 ($\delta^{18}O_{V\text{-}PDB} = -23.2‰$; $\delta^{13}C_{V\text{-}PDB} = -5.01‰$) and an in-house Carrara Marble standard ($\delta^{18}O_{V\text{-}PDB} = -1.84‰$; $\delta^{13}C_{V\text{-}PDB} = +2.03‰$) calibrated against international references NBS18 and NBS19. With the Carrara marble, the repeatability of the $\delta^{18}O$ and $\delta^{13}C$ measurements was 0.16‰ and 0.08‰ (2σ, n = 32), respectively.

With NBS18, the repeatability of the $\delta^{18}O$ and $\delta^{13}C$ measurements was 0.24‰ and 0.16‰ (2σ, n = 16), respectively. Replicate analyses of 13 foraminifera, 3 ostracod and 20 otolith samples generated replicate data within the repeatability of the method for both $\delta^{18}O$ and $\delta^{13}C$ (Agiadi et al., 2024b).

### 2.4 Biomarker analysis and sea surface temperature reconstruction

The biomarker analyses followed standard grinding, extraction, purification, and measurements detailed elsewhere (Besiou et al., 2024). Briefly, between 30 and 60 g of all 32 collected samples were dried and powdered. Lipids were extracted using a Soxhlet apparatus with a mixture of dichloromethane (DCM) and methanol (MeOH) (7.5:1; *v*:*v*) and pre-extracted cellulose filters. All extracts were evaporated to near dryness under $N_2$ flow with a TurboVap LV, obtaining the total lipid extracts (TLE). Subsequently, elemental sulfur was removed using 10% HCl-activated and neutralized, and solvent-cleaned Cu shreds. The TLE vials containing the activated Cu and magnetic rods were stirred overnight on a rotary plate. The samples were then filtered over a $Na_2SO_4$ column, dried, and desulfurized again until no reaction with Cu could be observed. A fraction of the TLE was separated into fractions by solid-phase $SiO_2$ gel column chromatography based on mixtures of solvents of increasing polarity. The apolar fraction was eluted using a mixture of *n*-hexane and DCM (9:1, *v*:*v*), the ketone fraction using DCM, and the polar fraction using a mixture of DCM/MeOH (1:1, *v*:*v*). The ketone fraction was analyzed using Gas Chromatography Mass Spectrometry (GC-MS), but the samples presented only seldom traces of alkenones, which could not be used for complementary SS reconstruction as initially intended. The polar fraction containing glycerol dialkyl glycerol tetraethers (GDGTs) was dried under $N_2$, dissolved in a 1 ml mixture of *n*-hexane (*n*-hexane)/isopropanol (IPA) (99:1, *v*:*v*), dispersed for ~30 s using an ultrasonic bath, then filtered over a 0.45 mm PTFE filter using a 1 ml syringe, and subsequently concentrated. The filtered polar fraction was measured using a Shimadzu HPLC, with two UHPLC silica columns (2.1 × 150 mm, 1.7 µm) in series, connected to a 2.1 × 5 mm pre-column coupled to an ABSciex 3200 Qtrap chemical ionization mass spectrometer (HPLC/APCIeMS) at SbiK-F. The column temperature was 30 °C and the flow rate was 0.2 ml × $min^{-1}$. The GDGTs were eluted isocratically using 18% B for 25 min, then a linear gradient to 35% B in 25 min, followed by a ramp to 100% B in 30 min, where B in *n*-hexane/isopropanol (9:1; *v*:*v*) and A is *n*-hexane. For each sample a 5 µl injection volume was used and GDGT detection was achieved through single ion monitoring for selected scanned masses: 1018, 1020, 1022, 1032, 1034, 1036, 1046, 1048, 1050, 1292, 1296, 1298, 1300, and 1302. The quantification of GDGTs was performed using the Analyst software and the peaks were integrated manually, more than twice for each sample to control for human-induced analytical bias. Because of the absence and/or traces of alkenones we were unable to estimate SST using the $U^{K'}_{37}$ paleothermometer. However, we found easily identifiable amounts of isoprenoidal (iso)GDGTs produced mainly by Archaea (Schouten et al., 2013) in open marine settings. Consequently, we applied $TEX_{86}$ paleothermometry (Kim et al., 2010; Schouten et al., 2002) to estimate the sea surface temperature (SST), as follows (Schouten et al., 2002) (Eq. 2):

$$TEX86 = \frac{[GDGT-2] + [GDGT-3] + [Cren']}{[GDGT-1] + [GDGT-2] + [GDGT-3] + [Cren']}, \quad (2)$$

where *GDGT-1*, *GDGT-2*, *GDGT-3* and *Cren'* are isoprenoid GDGTs. $TEX_{86}$ values were converted into SSTs using the calibration and recommendation of Kim et al. (2010) to apply $TEX_{86}^{H}$ > 15 °C for regions outside the polar and subpolar latitudes as follows (Eqs. 3 and 4):

$TEX^{H}_{86} = \log(TEX_{86})$ and the SST based on $TEX_{86}^{H}$ ($TEX^{H}_{86}$-SST) (3)

$TEX^{H}_{86}\text{-SST} = 68.4 \times (\text{GDGT index-2}) + 38.6$, ($r^2 = 0.87$, $p<0.0001$) (4)

where (Eq. 5):

$$GDGT\ index - 2 = log\frac{[GDGT-2]+[GDGT-3]+[Cren\prime]}{[GDGT-1]+[GDGT-2]+[GDGT-3]+[Cren\prime]}, \quad (5)$$

SST calculations based on $TEX_{86}^{H}$ have a calibration residual standard (1σ) error of ± 2.5 °C (based on 255 core-top sediments using Kim et al. (2010) calibration equation) (Agiadi et al., 2024b). The temperature error between sample replicates was ±0.3 °C. Thus, the propagated error in the temperature estimates is ±2.52 °C.

### 2.5 Organic matter content and sources

Productivity proxies produce different results depending on the setting and origin of the organic matter (Rühlemann et al., 1996). Relative changes in total productivity were estimated from the TOC content and the bulk $\delta^{13}C$, considering the sedimentary C/N ratio to distinguish between marine and terrestrial organic matter, as well as changes in the sedimentation rate that are expected between glacials and interglacials (El Frihmat et al., 2015). Sample preparation included grinding, removal of inorganic carbon (using 10 % HCl for 24 h at 40 °C), centrifugation (4 × at 2800 to 3000 rpm for 4 to 8 min), and sample drying (24 h at 40 °C). About 8 to 10 mg of sample were analyzed with a Flash EA 1112 that was coupled to a Thermo Fisher MAT 253 gas-source isotope ratio mass spectrometer at the SBiK-F. An uncertainty of 0.2 ‰ was indicated for measured $\delta^{13}C_{TOC}$ values by analyzing USGS 24 and IAEA-CH-7 standard materials on a daily basis and replicate measurements of reference materials and samples. The total organic carbon concentrations (in %) have been calculated by relating the signal size of the samples and the averaged signal size of the daily standards (USGS 24, n = 8). A typical error of ~0.5 % based on mass spectrometric analysis and maxi- mum differences of ~7 % in TOC contents of replicate measurements (including weighing uncertainties) was detected.

To evaluate the relative input of terrestrial organic matter for coastal versus marine organic matter we used Branched Isoprenoid Tetraether (BIT) index (Hopmans et al., 2004; Weijers et al., 2006), a biomarker-based proxy calculated as (Eq. 6) (Agiadi et al., 2024b):

$$BIT = [(GDGT-I) + (GDGT-II) + (GDGT-III)]/[(Crenarchaeol) + GDGT-I) + (GDGT-II) + (GDGT-III) \quad (6)$$

where *GDGT-I*, *GDGT-II* and *GDGT-III* are branched (br)GDGTs, which are components of bacterial cell membranes (particularly from Acidobacteria found in terrestrial, estuarine, and marine environments (Sinninghe Damsté et al., 2011; Weijers et al., 2006). *Crenarchaeol* is an isoGDGT and, together with brGDGTs, was analyzed and isolated as explained in section 2.4 (Agiadi et al., 2024b).

### 2.6 Foraminifera biomasses, ostracod and sponge spicule counts

The sediment samples were dry-sieved into seven size categories: < 125 μm, 125–150 μm, 150–200 μm, 200–250 μm, 250–315 μm, 315–400 μm, 400–500 μm, and > 500 μm. The < 125-μm residuals were excluded from the analyses following (Milker et al., 2017; van der Zwaan et al., 1990). We counted the number of planktonic and benthic foraminifera, ostracod valves, and sponge spicules in each size fraction. For foraminifera and ostracods, we only counted individuals whose shell or valve was at least half-preserved.

We estimated the planktonic foraminifera biomass (*pfb*) based on the empirical relationship between test size and protein mass (equivalent of biomass) developed by Schiebel and Movellan (2012) for 26 planktonic foraminifera species (Eq. 7):

$$M = 3.889 \times 10^{-4} \times d^{1.48} \quad (7)$$

where $M$ is the mass of the protein content (μg) and $d$ is the minimum diameter of the individual (μm). The benthic foraminifera biomass (*bfb*) was estimated using the relationship of Movellan et al. (2012) for *Ammonia tepida* (Eq. 8):

$$M = 5.537 \times 10^{-8} \times d^{2.941} \quad (8)$$

The total foraminifera biomasses (*fb*), *pfb*, and *bfb* (total and for each size class) are then calculated as the $M$ times the number of tests counted in the sample or fraction divided by the dry weight of the sediment sample in g. Ostracod and sponge spicules were counted at each sediment fraction and reported here as the number of valves or spicule fragments, respectively, per gram of sediment. Sponge spicule abundance is related to the abundance of sponge individuals (Łukowiak, 2020).

### 2.7 Sea surface salinity estimates

Foraminifera $\delta^{18}O$ records reflect both the temperature and the ambient oxygen isotopic composition of seawater ($\delta^{18}O_{sw}$) in which the shells precipitated. $\delta^{18}O_{sw}$, in turn, is influenced by global ice volume and ocean salinity. When the temperature (T) component is accounted for, foraminifera calcite $\delta^{18}O$ can be used to estimate past salinity changes, as $\delta^{18}O_{sw}$ covaries linearly with sea surface salinity (SSS). Both increase with evaporation and decrease with the addition of low-$\delta^{18}O$ freshwater (Legrande and Schmidt, 2006).

Building on this concept and in line with earlier studies (Kontakiotis et al., 2022; Vasiliev et al., 2019), we employed a multiproxy geochemical approach to estimate regional past SSS variability. To isolate $\delta^{18}O_{SW}$ from the measured foraminifera $\delta^{18}O$ values, we used $\delta^{18}O$ measurements from *Globigerinoides ruber* shells ($\delta^{18}O_{rub}$), the most surface-dwelling species. The temperature component was removed using the *Orbulina universa* low-light paleotemperature equation of Bemis et al. (1998), which is widely regarded as the most accurate for estimating paleo-SST in symbiotic planktonic foraminifera from subtropical settings in deep time (Williams et al., 2005).

Removing the temperature component from the $\delta^{18}O$ record using the paleotemperature equation enables the estimation of salinity. To account for the effect of continental ice volume, we utilized the Pleistocene eustatic sea-level curve of Rohling et al. (2014). Specifically, we linearly interpolated the sea-level curve to the studied time period and generated a record of

global $\delta^{18}O_{SW}$ changes associated with the melting of continental ice sheets during the Early–Middle Pleistocene. This was achieved by converting the sea-level data into mean ocean $\delta^{18}O$ changes and applying a 0.011‰ increase per meter of sea-level drop (Fairbanks and Matthews, 1978; Lea et al., 2002; Schrag et al., 1996). Furthermore, the $\delta^{18}O$ values of *G. ruber* were corrected for species-specific disequilibria from ambient seawater equilibrium ("vital effects") by applying a 0.48‰ adjustment (Peeters et al., 2002; Pracht et al., 2019). We then subtracted this component from the $\delta^{18}O_{SW}$ profile to derive the regional ice volume-free residual ($\delta^{18}O_{IVF\text{-}SW}$). The calculated $\delta^{18}O_{IVF\text{-}SW}$ values reflect changes in regional hydrography and are therefore considered to approximate local variations in sea surface salinity (SSS). To convert the $\delta^{18}O_{rub}$ signal into absolute SSS values, we applied the modern $\delta^{18}O_{SW}$–salinity relationship for the Mediterranean Sea of Pierre (1999) that refers to the surface waters with salinities greater than 36.2 (Eq. 9):

$$\delta^{18}O = 0.25\ (\pm 0.02) * S - 8.2\ (\pm 0.96) \qquad (9)$$

The uncertainty in salinity estimates arises from the propagation of errors associated with temperature estimates, $\delta^{18}O_{SW}$ reconstructions, and the $\delta^{18}O_{SW}$–salinity calibration equation. As demonstrated above, the error in the temperature estimates is 2.5 °C. Based on the $\delta^{18}O$ analytical error and the error associated with the paleotemperature equation, the propagation error for $\delta^{18}O$ is 0.63‰. Using the $\delta^{18}O_{SW}$ – salinity relationship from Pierre (1999), the average propagated uncertainty in salinity reconstruction is calculated to be ~5.4. In the accompanying graphs, the propagated salinity error was calculated for each sample individually, using the sample-specific $\delta^{18}O_{SW}$ residual.

### 2.8 Statistical analyses

To detect regime shifts, we first checked the time series of all the variables measured for normality using the Shapiro-Wilk test. For the variables whose values did not exhibit a normal distribution, we applied the L-method, which is based on the Mann-Whitney U test (Lanzante, 1996). For the variables whose values were normally distributed, we used the Sequential T-test Analysis of Regime-Shifts (STARS), which is additionally robust at the ends of the time series (Rodionov, 2004), setting Huber's weight parameter to 1 and the window size arbitrarily to 10. For both the L-method and the Rodionov's method, the *p*-value was set at 0.05.

Correlation was performed between: a) SST and all the $\delta^{18}O$ values (for bulk sediments, foraminifers, ostracods and otoliths); b) TOC (as a proxy of productivity and preservation of organic matter) and all the $\delta^{13}C$ values; c) SST and foraminifera biomasses (*fb*, *pfb*, *bfb*); d) TOC and the $\delta^{13}C$ in bulk sediment and foraminifers, against the foraminifera biomasses; e) SST and the ostracod weighted average body size; and f) TOC and the $\delta^{13}C$ in bulk sediment and foraminifers, against the ostracod body size. In all cases, we used the Spearman rank correlation coefficient (95% confidence level).

The above analyses were performed in R (version 4.3.3) (R Development Core Team, 2024) with the package *rshift* (Room et al., 2020).

### 2.9 Lifetime-average depth of mesopelagic fish

The foraminifera $\delta^{18}$O data represent the thermohaline gradient in the southeastern Aegean through time, and, with certain assumptions, are used here to estimate the position of the fishes in the water column. An exponential model is fitted using a log-linear regression on the $\delta^{18}$O values of foraminifera living at different depths to infer lifetime-average depths of the two common mesopelagic fish species, *Ceratoscopelus maderensis* and *Hygophum benoiti*, at each individual climatic cycle. The benthic foraminifera *Uvigerina peregrina* occupies the sea bottom and the depth used in our model is the paleodepth estimated in each sample based on the *%P/(B+P)* ratio. We assigned a distribution of 100–300 m to *Globoconella inflata*, assuming that this relatively deep-dwelling planktonic foraminifera is consistently most abundant at cool and nutrient-rich subsurface depths (Rohling et al., 2004; Schiebel and Hemleben, 2017). We finally assigned a distribution depth of 10–50 m to *Globigerinoides ruber*, assuming that this surface-dweller is most abundant at warmer and oligotrophic surface mixed-layer depths (Rohling et al., 2004; Schiebel and Hemleben, 2017).

Since direct measurements of depth ($y$) were not available for the planktonic foraminifera, we simulated the values within the ecological depth ranges of each species. For each species, depths were drawn from a uniform distribution over the respective depth ranges, assuming equal probability across the range.

We fit an exponential model using a log-linear regression where the realizations of our response variable $y_i$ represent the observed depths of any foraminiferal species. The response variable was log-transformed during modeling to establish an exponential relationship with $\delta^{18}$O ($x$) (Eq. 10):

$$\log(y_i) = \beta_0 + \beta_1 x + e_i \ , \ \ e_i \sim N(0, \sigma) \ , \ i = 1, \ldots, n \qquad (10)$$

where we assume that $\log(y_i)$ follows a normal distribution and that the linear predictor is made of an intercept $\beta_0$ and the relationship with $\delta^{18}$O. Separate models were fitted for glacial and interglacial cycles to account for potential differences in the $\delta^{18}$O-depth relationships between these periods.

Using the model at each individual MIS, we thus estimated the fish lifetime-average depth based on their otolith $\delta^{18}$O values. This model approach assumes that the thermal gradient remains the same within each MIS and that the water column is always well mixed. Although this is a simplified model of thermohaline conditions, the outputs offer a valuable perspective on the evolution of the lifetime-average depth and DVM patterns of mesopelagic fishes. The code for our model is available in (Fuster-Alonso et al., 2024).

## 3 Results

### 3.1 Paleodepths

The *%P/(P+B)* ratio ranges between 45% and 76%, and the 32 collected samples consequently deposited at the outer shelf (5 samples) and upper bathyal (27 samples) depths, with paleodepths $D$ estimates ranging between ~176 m and ~528 m. Although absolute paleodepth values based on *%P(P+B)* need to be taken very cautiously (Van Hinsbergen et al., 2007; van

der Zwaan et al., 1990), three main intervals with lower approximate values around ~200 m are recorded in the lower part of the section at heights between 40 and 60 cm, in the middle part of the section between 170 and 180 cm, and in the uppermost part of the studied deposits above 270 cm (Fig. 1). Overall, the highest upper bathyal depths are reached at three main intervals: below the height of 40 cm, between 70 and 160 cm, and between 190 and 270 cm.

### 3.2 Oxygen and carbon isotopic compositions

The $\delta^{18}O$ values of bulk sediments ($\delta^{18}O_{bulk}$) vary between −2.82 (LR30) and −0.70 ‰ (LR16) (Agiadi et al., 2024b). They are relatively higher overall up to height 160 cm, and lower thereafter. The $\delta^{13}C_{bulk}$ values range from −2.68 (LR25) to −0.96 ‰ (LR12) (Agiadi et al., 2024b). Lower values appear in general until LR16 and higher thereafter.

$\delta^{18}O_{ruber}$ values range from −0.62 (LR08) to 1.22 ‰ (LR01), $\delta^{18}O_{inflata}$ from 1.23 (LR17) to 2.19 ‰ (LR01), and $\delta^{18}O_{peregrina}$ from 1.51 (LR22) to 2.56 ‰ (LR30). The three species of foraminifera exhibit $\delta^{18}O$ values that reflect their depth-related ecology, with higher values in the benthic species *Uvigerina peregrina*, and lower $\delta^{18}O$ values in the surface mixed-layer species *Globigerinoides ruber* (Fig. 2). *Globoconella inflata* exhibit intermediate $\delta^{18}O$ values that are closer to those of *U. peregrina* (0.5 ‰ average gradient) than to those of *G. ruber* (1.7 ‰ average gradient), then confirming that *G. inflata* mineralized at cooler/deeper water depths than *G. ruber*. *Globigerinoides ruber* and *U. peregrina* exhibit an average gradient of 1.9 ‰ between surface and bottom waters. *Uvigerina peregrina*, *G. inflata* and *G. ruber* show similar overall variation trends throughout the section, but with discrepancies notably recorded between *G. ruber* and the two other species.

We were only able to find valves of the ostracod genus *Bairdopilata* at the upper part of the section. $\delta^{18}O_{baird}$ ranges from 1.93 (LR28) to 5.69 ‰ (LR30).

For the fishes, $\delta^{18}O_{benoiti}$ ranges from 2.56 (LR28) to 7.35 ‰ (LR02), and $\delta^{18}O_{mader}$ ranges from −3.3 (LR16) to 3.50 ‰ (LR10). There is no significant correlation between otolith weight and $\delta^{18}O$. $\delta^{13}C_{ruber}$ ranges from −0.18 (LR02) to 1.13 ‰ (LR19), with lower values until LR07. $\delta^{13}C_{inflata}$ ranges from −0.2 (LR17) to 0.58 ‰ (LR07), and $\delta^{13}C_{peregrina}$ ranges from −0.89 (LR16) to −0.3 ‰ (LR10). Ostracod $\delta^{13}C_{baird}$, only measured in the upper part of the section, ranges from −1.18 (LR28) to −0.61 ‰ (LR25). For the fishes, $\delta^{13}C_{benoiti}$ ranges from −5.25 (LR32) to 0.99 ‰ (LR09), with generally more negative values in the upper part of the section, and $\delta^{13}C_{mader}$ ranges from −6.70 (LR07) to 2.92 ‰ (LR16). The distributions of the $\delta^{13}C_{mader}$ and $\delta^{13}C_{benoiti}$ values are shown in Fig. S1. There is significant correlation between otolith weight and otolith $\delta^{13}C$ for both *Hygophum benoiti* (rho = 0.45, p = 0.04) and *Ceratoscopelus maderensis* (rho = 0.80, p = 0.0003). The different foraminifera and fish species show distinctive patterns of $\delta^{13}C$ and $\delta^{18}O$ (Fig. S2).

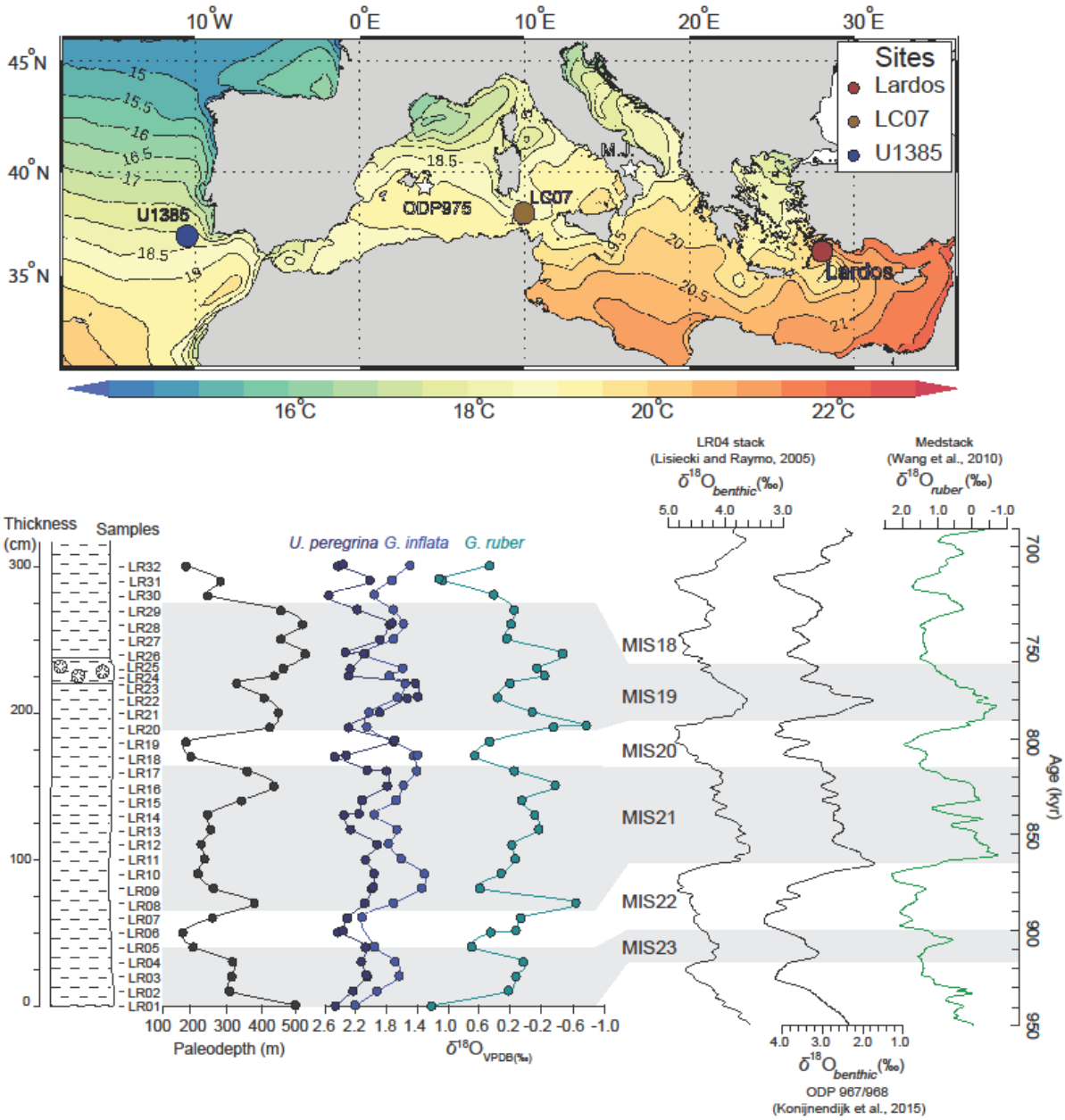


**Figure 1. Map of the Mediterranean region with present-day SST (Minnett et al., 2019) and the location of Lardos (our study area), LC07 (Martínez-Dios et al., 2021), U1385 (Rodrigues et al., 2017), ODP975 (Quivelli et al., 2020, 2021), and M.J. Montalbano Jonico (Marino et al., 2020; Peral et al., 2020). Paleodepth estimates based on the *%P/(B+P)* ratio and proposed correlation between foraminifera $\delta^{18}$O records of the Lardos section and open ocean $\delta^{18}$O reference records: the LR04 benthic global $\delta^{18}$O stack (Lisiecki and Raymo, 2005), the benthic Eastern Mediterranean $\delta^{18}$O compilation data from Ocean Drilling Program (ODP) Sites 967 and 968 (Konijnendijk et al., 2015), and the planktonic (*Globigerinoides ruber*) $\delta^{18}$O Medstack (Wang et al., 2010). The paleodepth changes (with a glacio-eustatic component) and the coincidence of successive positive and negative excursions in the $\delta^{18}$O records allow refining the chronostratigraphy previously published for the section (Titschack et al., 2013). This revised age model reveals the identification of six distinct isotopic stages between MIS 23 and MIS 18, including three interglacials (gray areas) and three glacials (white areas).**

### 3.3 Refining the age model

We used the new local oxygen isotope stratigraphy and paleodepth estimates from this work to refine the published chronostratigraphy of the studied deposits (Titschack et al., 2013). At heights of 30 to 40 cm (LR04–05), the $\delta^{18}$O values of all three species of foraminifera increase and the paleodepth shows a sharp decrease. Such changes are proposed to correlate with those occurring in the LR04 global (Lisiecki and Raymo, 2005) and Mediterranean (Konijnendijk et al., 2015) benthic $\delta^{18}$O stacks, and with that occurring in the planktonic foraminifera Mediterranean $\delta^{18}$O Medstack (Wang et al., 2010) between MIS 23 and MIS 22 (Fig. 1). In this re-examination of the age model of the Lardos section, we assign the MIS 22/21 termination (866 kyr; Lisiecki and Raymo, 2005) to the height of 65 cm, in accordance with Titschack et al. (2013). Such a level, characterized by a change in the slope in all foraminifera $\delta^{18}$O records and a sharp increase in paleodepth, is proposed in agreement with those occurring in open-ocean reference records (Fig. 1). We also delineate the MIS 21/20 (814 kyr) and MIS 20/19 (790 kyr) terminations to the heights 165 (LR17–18) and 185 cm (LR19–20), respectively. Within the sedimentary interval that we allocate to MIS 20, and that shows shallower paleodepths, both *U. peregrina* and *G. ruber* exhibit increasing $\delta^{18}$O values similar to those of open-ocean reference records (Fig. 1). Finally, we assign the MIS 19/18 termination (761 kyr) to the height of 275 cm (LR29–30), in accordance with the previously published chronostratigraphy (Titschack et al., 2013). Such a level shows increasing $\delta^{18}$O values in all foraminifera taxa, similar to the open-ocean records, and a sharp decrease in paleodepth.

Based on these tie-points, we estimate the average sedimentation rates for the deposits within each climate cycle in the MIS 22–19 interval. The sedimentation rates within MIS 22 and MIS 19 are then linearly extrapolated to MIS 23 and MIS 18, respectively. According to this refined age model, the samples analyzed in this study were deposited within the MIS 23–18 interval between ~923 and ~756 kyr. The age estimate of each sample (Agiadi et al., 2024b) is used for the results and discussions on the observed changes during the MPT at Lardos.

### 3.4 $TEX^{H}_{86}$-SST and SSS

SST ranges from 19.2 to 26.1 °C (Fig. 2). From 923 to 864 kyr, SST decreases to 20.5 °C. The interval 861–858 kyr exhibits higher temperature, but afterwards it is low until 820 kyr, when it starts to increase to a maximum of 24.4 °C around 798 kyr. Between 788 and 762 kyr, SST shows intermediate, but rather stable values fluctuating around 23 °C, and then increases until 756 kyr to 25.9 °C.

SSS ranges from 31.9 to 42.3 (Fig. 2). From 923 to 864 kyr, SSS decreases to 31.9, but 861–858 kyr experiences the highest SSS values. Afterwards, SS decreases again and shows intermediate values after 760 kyr.

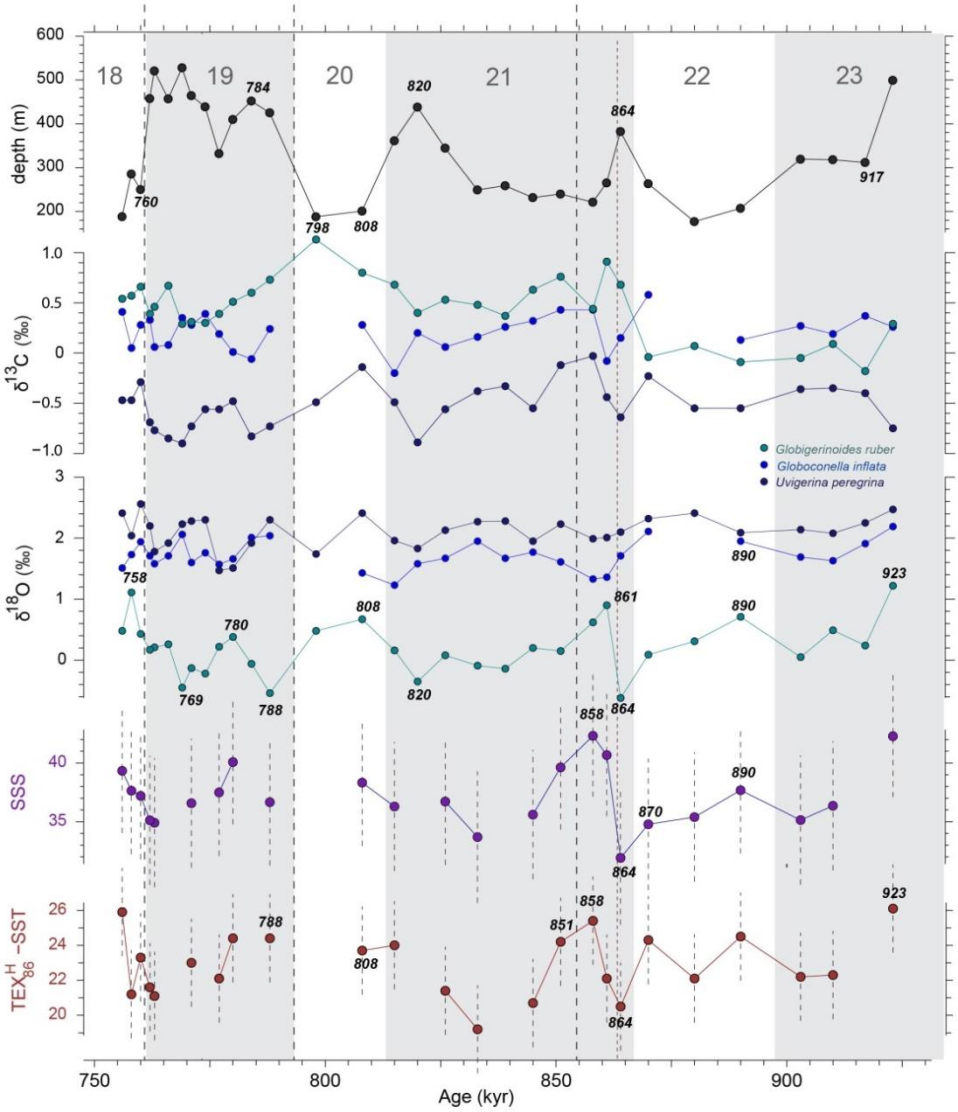


**Figure 2. Paleoclimatic and paleoceanographic conditions at Lardos. Paleodepth estimates based on the *%P/(B+P)* ratio. $\delta^{18}$O and $\delta^{13}$C values of the surface-dwelling planktonic foraminifera *Globigerinoides ruber*, the deeper-dwelling planktonic foraminifera *Globoconella inflata*, and the benthic foraminifera *Uvigerina peregrina*. $TEX_{86}$-derived sea surface temperature (SST) and salinity (SSS) data, where bars are used to visualize the ±2.5 °C error. The three red wide-dashed vertical lines indicate the three regime shifts identified using the STARS algorithm (TOC, $\delta^{18}O_{peregrina}$ and $\delta^{18}O_{ruber}$ at 760 kyr; $\delta^{13}C_{peregrina}$ and the ostracod weighted average body size at 788 kyr; and $\delta^{13}C_{ruber}$ at 851 kyr), whereas the narrow-dashed line shows the regime shift identified using the L-method (ostracod weighted average body size at 864 kyr). Grey-shaded areas represent interglacials, whereas white areas are glacials; the number of each MIS is indicated on top. Italicized numbers show the ages corresponding to each data point.**

### 3.5 Organic content in the sediments

The BIT index is lower in the older part of the section (i.e., greater input of marine organic matter), with a minimum of 0.45 at 870 kyr (Fig. 3). It then increases (toward more terrestrial organic matter) to reach a maximum of 0.80 at 815–808 kyr and remains high in the younger part of the section. TOC ranges from 0.152 to 0.266% and TN from 0.027 to 0.042%, making the C/N ratio range from 5.14 to 7.27 (Fig. 3). From 923 kyr, both TOC and TN increase to reach 0.266% and 0.042%, respectively, at 864 kyr. In the interval 861–820 kyr, they show relatively high values, which then decrease to a minimum at 798 kyr of 0.180 and 0.032%, respectively. Intermediate values appear from 788 to 762 kyr, and then low values for both TOC and TN until 756 kyr.

### 3.6 Foraminifera biomass

The foraminifera biomass is mostly composed of plankton (*pfb*), which is much greater than benthos (*bfb*) at all levels: the minimum is found at 756 kyr (88.3 µg/g for *fb*, 58.8 µg/g for *pfb*, and 29.4 µg/g for *bfb*), whereas the maximum biomass is found at 766 kyr (1763.3 µg/g for *fb*, 1518.2 µg/g for *pfb*, and 245.1 µg/g for *bfb*) (Fig. 4). For both *pfb* and *bfb*, the contributions of the size classes to the total biomass varies greatly (Figs. S3 and S4). From 923 to 880 kyr, both *pfb* and *bfb* are low, and then they increase to peak at 861 kyr (867.7 µg/g and 240.4 µg/g, respectively). They remain high until 815 kyr, and then decrease until 788 kyr (minima are 303.5 µg/g at 798 kyr and 60.7 µg/g at 788 kyr, respectively). In general, *bfb* covaries with *pfb*, with two exceptions, at 774 and 769 kyr, where *bfb* is particularly low (77.6 and 66.5 µg/g).

### 3.7 Ostracod and sponge spicule counts

The total ostracod abundance ranges from 2 valves/g at 774 kyr to 25 valves/g at 758 kyr (Fig. 4). From 923 to 903 kyr, the medium–high abundance is driven by ostracod valves in the 150–200 µm size-class. The overall number of valves then decreases, and high values are found again from 861 to 820 kyr, when their abundance increases across size classes. The abundance after that point fluctuates between low and medium levels, and only shows maximum values at 758 kyr due to highs in the >500, 315–400, and <200 µm size-classes.

The number of sponge spicule fragments per gram of sediment range from 2 at 880 kyr to 18 at 826 kyr (Fig. 4). The weighted average size of the ostracod valves ranges from 159 µm at 903 kyr to 241 µm at 774 kyr. Broadly, similar to ostracod abundance and foraminifera biomass, the values are generally relatively high around 861–820 kyr. The weighted average size of the spicules ranges from 149 µm at 760 kyr to 318 µm at 758 kyr.

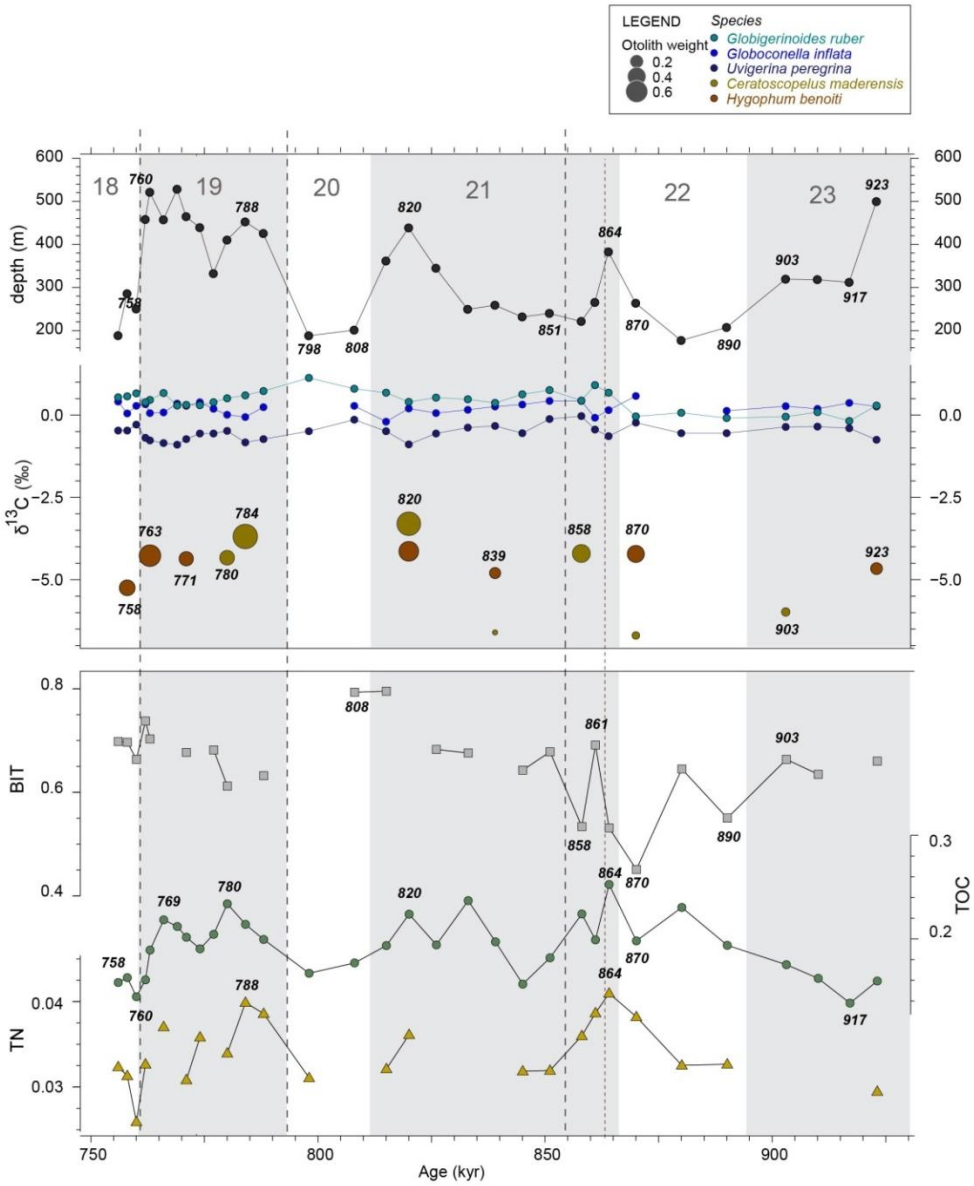


**Figure 3. Organic matter and productivity proxy records at Lardos. Paleodepth estimates based on the *%P/(B+P)* ratio. $\delta^{13}$C values of the surface-dwelling planktonic foraminifera *Globigerinoides ruber*, the deeper-dwelling planktonic foraminfera *Globoconella inflata*, and the benthic foraminifera *Uvigerina peregrina*. The $\delta^{13}$C of the fish otoliths results from the $\delta^{13}$C of the dissolved inorganic carbon in the ambient water (indicated here at different depths by the foraminifera $\delta^{13}$C values) and the $\delta^{13}$C of their diet items. Ultimately, the $\delta^{13}$C of otoliths is a proxy of the metabolic rate of the fish. The totalotal organic carbon (TOC) and total nitrogen (TN) contents reflect productivity, and the Branched Isoprenoid Tetraether (BIT) index reflects the source of the organic matter in the sediment (which increases with terrestrial influx). Grey-shaded areas represent interglacials, whereas white areas are glacials; the number of each MIS is indicated on top. Italicized numbers show the ages corresponding to each data point.**

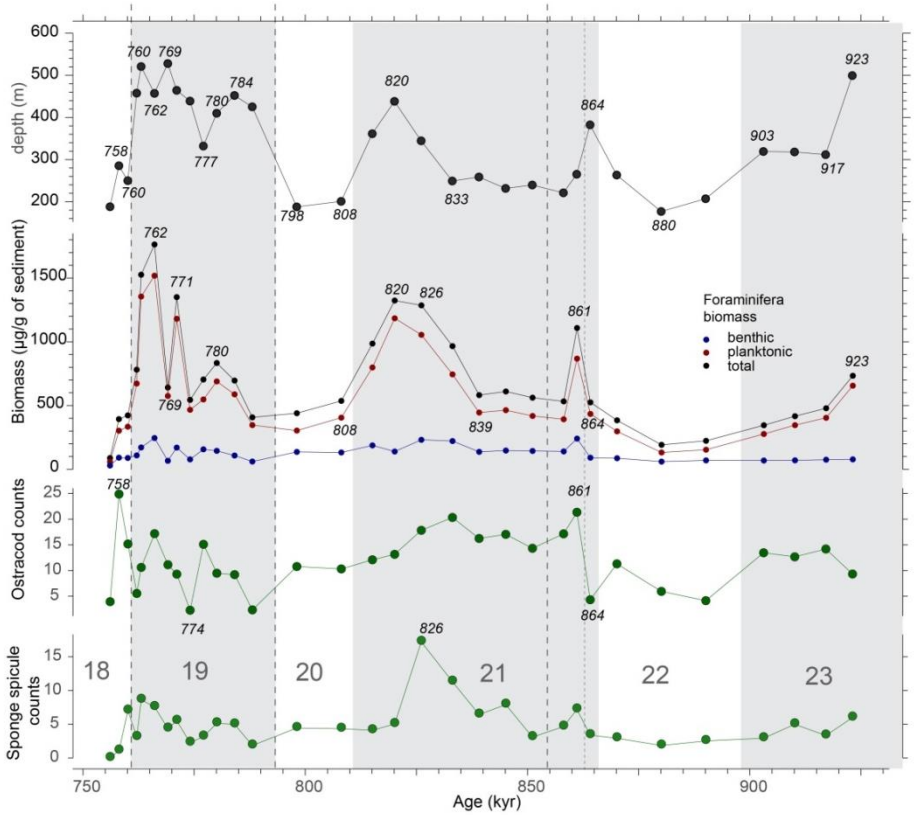


**Figure 4. Planktonic foraminifera biomass, ostracod and sponge spicule counts at Lardos. Paleodepth estimates based on the *%P/(B+P)* ratio. Grey-shaded areas represent interglacials, whereas white areas are glacials; the number of each MIS is indicated on top. Italicized numbers show the ages corresponding to each data point.**

### 3.8 Fish average depth in the water column

Our model shows a steeper $\delta^{18}O$ gradient during interglacials than during glacials, predicting greater depth values for fish (Fig. 5). Based on the model results, the lifetime-average depth ranges from 474 m at 870 kyr to 933 m at 839 kyr for *Hygophum benoiti* and from 330 m at 903 kyr to 1502 m at 858 kyr for *Ceratoscopelus maderensis* (Fig. 6). We could not detect a significant correlation between the modeled fish depth and otolith weight, which suggests that fish depth is not controlled by life history in the same way throughout the studied interval for either species. Additionally, we did not find any significant correlation between the modeled depth and SST, TOC, or $\delta^{13}C_{bulk}$.

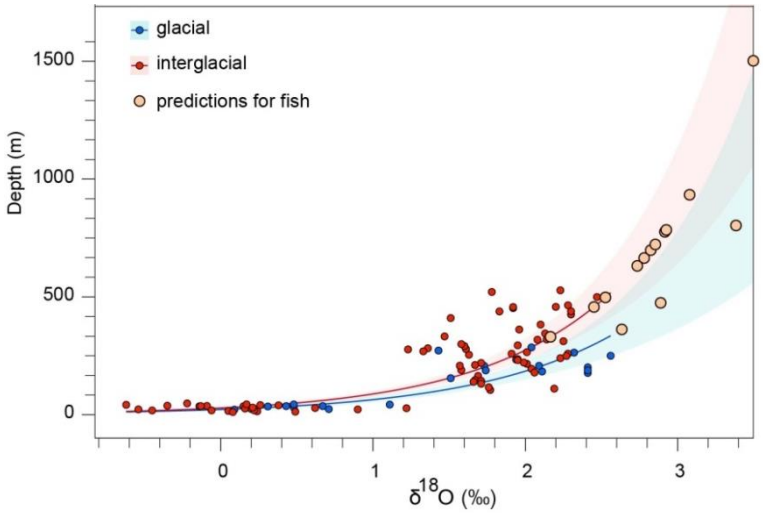


**Figure 5. Fitted regression for glacial and interglacial climate cycles with extrapolated fish predictions and 95% confidence intervals.**

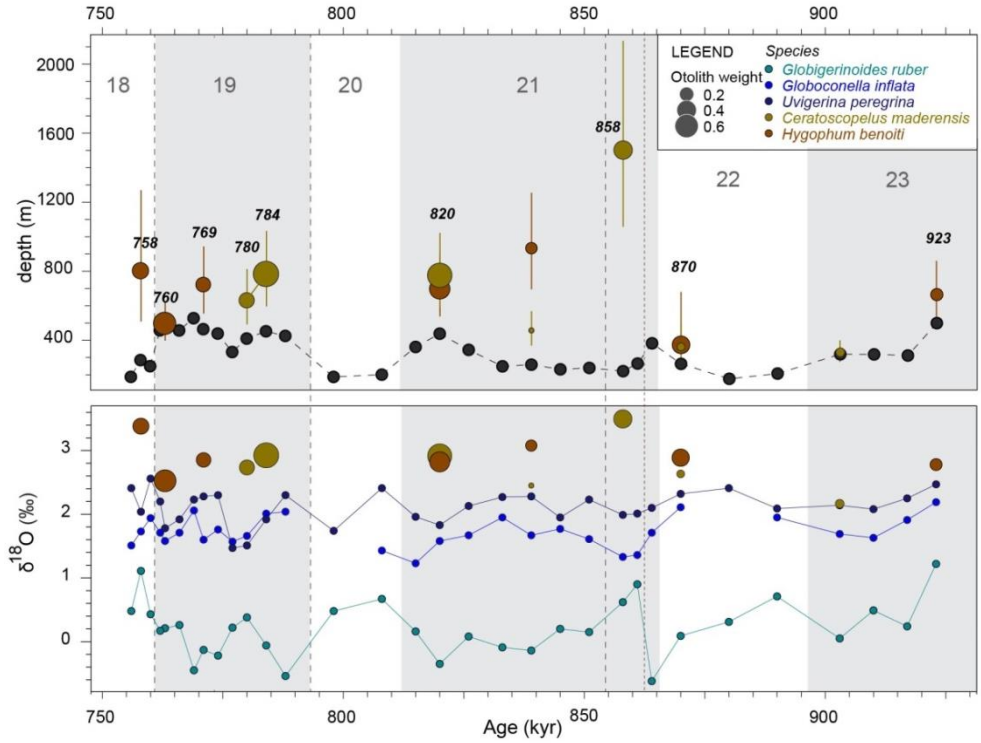


**Figure 6. Paleodepth and modeled lifetime-average depths where the two mesopelagic fish species lived in the study area, obtained from the $\delta^{18}$O values in their otoliths by modeling the thermohaline gradient using the $\delta^{18}$O values of the different species of foraminifera. The circle diameter scales with otolith weight, reflecting fish size, whereas the vertical lines indicate the depth ranges. Grey-shaded areas represent interglacials, whereas white areas are glacials; the number of each MIS is indicated on top. Italicized numbers show the ages corresponding to each data point.**

### 3.9 Regime shifts and covariance

Positive values of the Regime Shift Index (RSI) indicate the presence of regime shifts (95% confidence level) for: a) TOC, $\delta^{18}O_{peregrina}$ and $\delta^{18}O_{ruber}$ at 760 kyr (RSI = 0.940, 1.437 and 0.265, respectively); b) $\delta^{13}C_{peregrina}$ and the ostracod weighted-average body size at 788 kyr (RSI = 0.583 and 0.231, respectively); and c) $\delta^{13}C_{ruber}$ at 851 kyr (RSI = 0.788). Additionally, a regime shift was found using the Lanzante method for the sponge weighted average size at 864 kyr (p = 0.006).

Regarding foraminifera biomasses, a medium correlation is detected between: a) SST and benthic foraminifera biomass (rho = −0.44; p = 0.03); b) $\delta^{13}C_{ruber}$ and benthic foraminifera biomass (rho = 0.45; p = 0.01); c) $\delta^{13}C_{inflata}$ and total foraminifera biomass (rho = −0.42; p = 0.02), planktonic foraminifera biomass (rho = −0.45; p = 0.014), and the benthic foraminifera biomass (rho = −0.44; p = 0.014); d) $\delta^{13}C_{peregrina}$ and the total foraminifera biomass (rho = −0.47; p = 0.007) and the planktonic foraminifera biomass (rho = −0.53; p = 0.002); and e) $\delta^{13}C_{bulk}$ and the total foraminifera biomass (rho = 0.52; p = 0.003), the planktonic foraminifera biomass (rho = 0.52; p = 0.003), and the benthic foraminifera biomass (rho = 0.42; p = 0.019). Medium correlation is also found between $\delta^{13}C_{peregrina}$ and the ostracod weighted average body size (rho = 0.40; p = 0.02).

## 4 Discussion

### 4.1 Climate, productivity and organic carbon burial

The unique SST reconstruction for the Eastern Mediterranean that is presented here is not nearly as resolved in time as the equivalent from deep-sea cores in the Western Mediterranean and the Atlantic due to the large difference in sedimentation rates between the sites, highlighting the importance of obtaining SST records from deep-sea drilling sites in the Eastern Mediterranean. The SST in the study area is consistently warmer than those in the Central and Western Mediterranean, with higher mean SST values found in all climate cycles, between MIS 23 and 18 (Table S1; Fig. 7), as observed today (Minnett et al., 2019). The glacial–interglacial SST amplitude is similar (~5 °C) at both Site LC07 and Lardos, but very different from that recorded at the Atlantic Site U1385 (Fig. 7). The two-fold smaller temperature changes observed at the Mediterranean sites indicate that the basin responded to the global climate change during the MPT, but the recorded temperatures must have also been influenced by the semi-enclosed configuration of the Mediterranean Sea. The SST values from Lardos are also higher than those reconstructed from Site LC07. Part of this difference can be explained by a system similar to the present-day one, where the Eastern Mediterranean is ~2 °C warmer than the Central Mediterranean is (Minnett et al., 2019). Another part of the difference can also be explained by the different proxies used to obtain the SST estimates, i.e. $TEX_{86}$ for Lardos and $U^{K'}_{37}$ for Site LC07. $TEX_{86}$ generally overestimates SSTs by 2–6 °C (Kim et al., 2015), whereas $U^{K'}_{37}$ tends to underestimate SSTs by 2–4 °C (Tierney and Tingley, 2018). Importantly, based on the TOC content of the analyzed samples, we could not capture any of the sapropels (Martínez-Dios et al., 2021) in the study area. Four paleoceanographic regimes

were identified within the studied time interval in the southeastern Aegean, based on the regime shift analysis: a) 923–858 kyr; b) 851–798 kyr; c) 788–762 kyr; and d) 760–756 kyr.

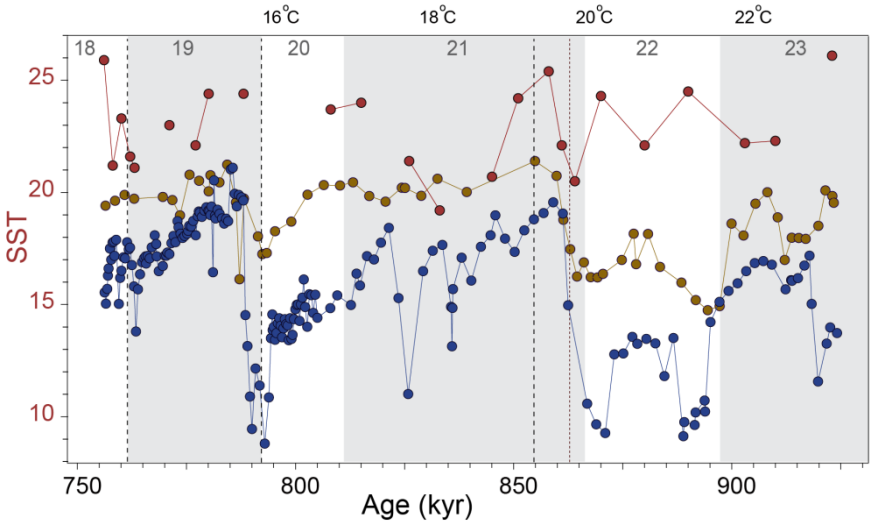


**Figure 7. SST time series for: Lardos (this study), Site LC07 (Martínez-Dios et al., 2021), Site U1385 (Rodrigues et al., 2017), ODP Site 975 (Quivelli et al., 2020, 2021), and M.J. Montalbano Jonico (Marino et al., 2020; Peral et al., 2020). The mean SSTs for all the localities are shown in (Agiadi et al., 2024b).**

#### 4.1.1 923–858 kyr

The interval between 923 and 858 kyr includes the MIS 23 interglacial, the MIS 22 glacial, and the early part of the MIS 21 interglacial. SST declines from MIS 23 to MIS 22 and increases in MIS 21 (Fig. 2). TOC (and TN) increase throughout the study interval (Fig. 3). Planktonic and benthic foraminifera biomasses are low in MIS 23 and even lower in MIS 22, but increase drastically in MIS 21 (Fig. 4). Overall, stable high values appear for this interval in $\delta^{13}C_{bulk}$, and $\delta^{13}C_{peregrina}$ shows intermediate values (Fig. 3). $\delta^{13}C_{inflata}$ decreases in the 864–858 kyr interval. In contrast, $\delta^{13}C_{ruber}$ values are higher in MIS 23 and MIS 21, and lower in MIS 22.

The TOC and $\delta^{13}C$ values of the bulk sediment and foraminifera shells reflect changes in productivity as well as enhanced organic carbon burial (Jing et al., 2024; Spezzaferri, 1995). Benthic foraminifera accumulation rates from deep-sea drilling sites are often used to estimate changes in productivity (Diester-Haass et al., 2018). Our results suggest that productivity during the 923–864 kyr interval fluctuates with climate, as reflected by the values of $\delta^{13}C_{ruber}$ (Fig. 3) and the foraminifera biomasses (Fig. 4). In contrast, organic carbon burial declines during the 923–864 kyr interval, since the benthic $\delta^{13}C_{peregrina}$ values remain approximately the same. The regime shift in the sponge weighted average size at 864 kyr is coupled with a large increase in BIT (Fig.3) and foraminifera biomasses, and a decrease in $\delta^{18}O_{inflata}$ and $\delta^{18}O_{peregrina}$ (while $\delta^{18}O_{ruber}$ remains at the same levels), suggesting lengthening of the thermal gradient in the water column associated with the influx of terrestrial organic matter (i.e., higher BIT) that benefited secondary production.

#### 4.1.2 851–798 kyr

This interval encompasses most of the MIS 21 interglacial, after the SST maximum at 858 kyr (Fig. 2), and the MIS 20 glacial. The regime shift in $\delta^{13}C_{ruber}$ denotes a paleoenvironmental or ecosystem change in Lardos at 851 kyr. The $\delta^{13}C$ of foraminifera is a proxy of the $\delta^{13}C$ of dissolved inorganic carbon in the seawater where shell calcification took place, which increases with primary productivity, influx of terrestrial organic matter and water mixing (Ravelo and Hillaire-Marcel, 2007). The lack of regime shifts in $\delta^{13}C_{inflata}$ and $\delta^{13}C_{peregrina}$ implies that surface waters were the most affected by the change. BIT increases to a maximum around the MIS 21/MIS 20 transition (Fig. 3), reflecting more terrestrial organic matter, and both *pfb* and *bfb* increase at the same time.

#### 4.1.3 788–762 kyr

The interval between 788 and 762 kyr includes the entire MIS 19 and is characterized at Lardos by a regime shift in $\delta^{13}C_{peregrina}$ and the ostracod weighted-average body size. The $\delta^{13}C_{peregrina}$ values during this interval are generally the lowest, while ostracods show a drastic decline in body size with an almost complete absence of sizes > 500 μm. From 780 kyr toward MIS 18, SST indicates a cooling trend (Fig. 2), which was also detected along the Iberian margin and has been related to a progressive southward migration of the polar front (Girone et al., 2023). A decreasing trend is also evident in SSS (Fig. 2) from 780 to 762 kyr. Higher foraminifera (planktonic especially) biomasses are observed throughout the 788–762 kyr interval, as expected since they are significantly correlated with $\delta^{13}C_{peregrina}$. The lowest values are also observed for $\delta^{13}C_{bulk}$. Therefore, we propose that higher productivity during MIS 19 was accompanied by enhanced organic carbon burial to explain the concurrent higher planktonic foraminifera biomass and low $\delta^{13}C_{peregrina}$ and $\delta^{13}C_{bulk}$ values. Higher primary productivity and organic carbon burial have been reported at least for the early part of MIS 19 in the Western Mediterranean as well (ODP Site 975; (Marino et al., 2022; Quivelli et al., 2020).

#### 4.1.4 760–756 kyr

The interval from 760 to 756 kyr captures the oldest part of MIS 18 at Lardos. SW Europe winter precipitation and the East Asia summer monsoon strength peaked during MIS 18, contributing to the expansion of the Northern Hemisphere ice sheets (Sánchez Goñi et al., 2023). In our study area, the paleoceanographic conditions change at the MIS19–MIS18 transition, as captured by regime shifts in TOC, $\delta^{18}O_{peregrina}$ and $\delta^{18}O_{ruber}$. TOC shows low values (Fig. 3), whereas $\delta^{18}O_{peregrina}$ and $\delta^{18}O_{ruber}$ show higher values than in MIS 19 (Fig. 2). However, SST and SSS are not higher than in the early part of MIS 19, but the estimated paleodepth is shallower at this time (Fig. 2). The sea-level change that occurred during MIS 18 and the shallowing of the Lardos area likely explain the observed regime shift.

### 4.2 Thermohaline gradient

The thermohaline gradient is inferred from the $\delta^{18}O_{ruber}$ (corresponding to surface waters), $\delta^{18}O_{inflata}$ (intermediate waters), and $\delta^{18}O_{peregrina}$ (bottom waters) values, considering the paleodepth in the study area (Fig. 2). The gradient between these values is steeper in MIS 23–MIS 22 but attenuates in MIS 21. In the late part of MIS 21, a short warmer period occurs around 820 kyr (Fig. 2), but the differences between the foraminifera $\delta^{18}O$ values are maintained despite the greater paleodepth, suggesting that the thermohaline gradient is less steep than before. During MIS 20 and MIS 18, the gradient is smaller but this can be explained by the shallower depth during the glacials (Fig. 2). Our model produces steeper thermohaline gradients during interglacials than during glacials (Fig. 5), as expected due to the lower thermal conductivity of water masses.

### 4.3 Responses across the food web

Planktonic and benthic foraminifera biomass changes closely follow the paleodepth changes recorded in the study area (Fig. 4). Since paleodepths exceed the euphotic zone depth at all times, this observation is unlikely to be due to increased accumulation of shells on the seabed with increasing depth, but rather a genuine signal. Accordingly, higher foraminifera biomass is observed during interglacials than glacials, and this is confirmed by the ostracod and sponge abundances (Fig. 4). Additionally, the planktonic foraminifera in MIS 21 and MIS 19 interglacials are the largest overall, with the > 500 μm size fraction increasing in those intervals. Larger shell sizes in planktonic foraminifera are typically associated with temperature and/or primary productivity conditions that are close to the optimum values for these organisms (Schmidt et al., 2004). Therefore, we can safely assume overall higher secondary production during interglacials.

Otolith $\delta^{13}C$ in conjunction with foraminifera $\delta^{13}C$ is informative of how the metabolic rate of fishes changes through time (Agiadi et al., 2024a). In this case, no important changes in the otolith $\delta^{13}C$ values of the two fish species are observed over time. An exception is the slight drop in $\delta^{13}C_{benoiti}$ in MIS 18, which is only occurred from one point. In general, a lower $\delta^{13}C_{oto}$ reflects a higher metabolic rate or a change to higher trophic-level (and therefore lower $\delta^{13}C$) food items (Chung et al., 2019b). Here, overall, the larger otolith specimens exhibit higher $\delta^{13}C$ values, suggesting that, as the animals grew, they consumed fewer and/or switched to lower-trophic–level items. A possible explanation could be that younger individuals consumed much, primarily detritus, whereas adults became more selective, consuming mesozooplankton.

### 4.4 Changes in fish diel vertical migration and implications for the carbon pump

The $\delta^{18}O$ values of both mesopelagic fish species are consistently greater than those of foraminifera, which indicates that these fishes experienced much cooler and/or saltier seawater temperatures on average. Otolith $\delta^{18}O$ is a function of seawater temperature and varies according to the lifestyle of the species in question (Kalish, 1991b, a). Both *Ceratoscopelus maderensis* and *Hygophum benoiti* perform DVM. The fact that $\delta^{18}O_{benoiti}$ and $\delta^{18}O_{mader}$ fluctuate between much more positive and almost the values of $\delta^{18}O_{peregrina}$ suggests that they spend only part of their day in the study location, migrating

from greater depths. Furthermore, with the present data, the $\delta^{18}O_{benoiti}$ and $\delta^{18}O_{mader}$ variability cannot be related to the $\delta^{18}O_{foram}$ or $\delta^{18}O_{bulk}$ variability, nor the SST changes. Particularly, for *Ceratoscopelus maderensis*, this variability shows high amplitude, suggesting that this species changed its DVM pattern and/or its depth distribution within the studied time interval. Today, the common, extant species *Ceratoscopelus maderensis* shows different depth ranges in the Atlantic Ocean (Badcock and Merrett, 1976; Killen et al., 2010; Kinzer and Schulz, 1985) than in the Mediterranean Sea, and even within the latter (up to 1480 m in the Levantine Sea (Goren and Galil, 2015), but up to 2500 m in the Ionian Sea (Olivar et al., 2012)). Our $\delta^{18}O$–depth model estimates of the lifetime-average depth of the two mesopelagic fishes show high variability.

In MIS 23–22, *Ceratoscopelus maderensis* (indicated by small otolith specimens corresponding to young individuals) are distributed on average at depths of 330 m (Fig. 6), which is at the very shallow end of the present-day distribution of this species, suggesting that the individuals (at least the young ones) were performing DVM and/or occupying shallow depths (Fig. 8), as observed today in the Mediterranean (Olivar et al., 2012). The modeled depth of *Hygophum benoiti* is deeper in MIS 23, but the same in MIS 22, as is the case for *C. maderensis*. However, we cannot interpret this as an absence of DVM by that species in MIS 23, because we have only examined a few specimens per species as replicates. A greater number of otolith specimens should be analyzed per sampling unit to reconstruct the frequency distribution of the lifetime-average depths of each species to be able to confidently exclude DVM. Large adults of both species are distributed at shallower depths (776 and 698 m, respectively) in the later part of MIS 21, and the same pattern is observed in MIS 19.

A drastic shift to greater depth (model estimate: 1502 m) is observed for *Ceratoscopelus maderensis* in the initial part of MIS 21 (Fig. 6), which similarly indicates slowing down of DVM and/or drastic shift of these fish to much greater mesopelagic depths than before (Fig. 8). These two alternative explanations would have opposite effects on the biological carbon pump and therefore on carbon sequestration and burial. If the depth distribution range of the fishes simply expanded to greater depths but continued to perform DVM, then we would expect to see an increase in organic carbon burial at the time, which is not observed on TOC or $\delta^{13}C$ data (Fig. 2). In contrast, we support that the DVM capacity of fishes was hindered by the warming that occurred in the early part of MIS 21, resulting in a reduction in the biological carbon pump efficiency (Fig. 8) and relatively stable carbon burial despite the enhanced terrestrial input (increased BIT; Fig. 3) and subsequent interglacial.

The rather great depths for the distribution of juveniles of both *C. maderensis* (457 m) and *H. benoiti* (933 m) around the middle part of MIS 21 reinforce the interpretation of a reduction in DVM, and further signal a gradual re-establishment of regular DVM patterns (replicate data confirming this are available in (Agiadi et al., 2024b)). This event was concurrent with a shift in global and Mediterranean SST (Fig. 7). Although higher resolution and more sites are necessary to investigate the extent of this phenomenon, our results support the hypothesis that warming reduces the biological carbon pump efficiency by restricting mesopelagic zone ecosystem functioning (Boscolo-Galazzo et al., 2021).

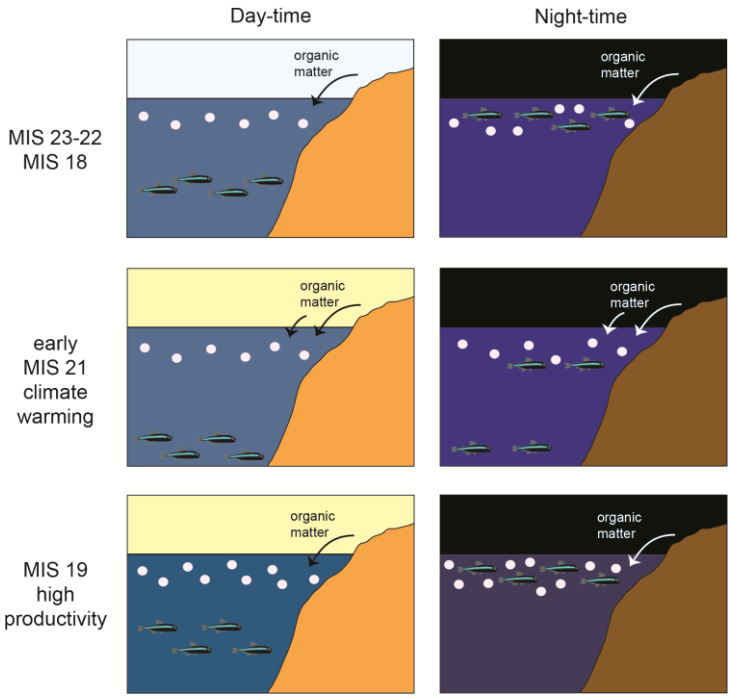


**Figure 8. Schematic representation of the changes in diel vertical migration patterns during the Middle Pleistocene Transition interval of the study (MIS 23–18), as suggested by our data.**

## 5 Conclusions

We employed here a multiproxy approach to reconstruct the paleoceanographic conditions and the response of the pelagic ecosystem to their changes between 923 and 756 kyr in the Eastern Mediterranean. Glacial–interglacial changes in the Pleistocene tested the limits of marine ecosystem resilience in multiple ways, resulting in distribution range shifts, ecophenotypic adaptations, and ultimately species extinctions (Agiadi et al., 2011, 2018, 2023; Porz et al., 2024). During the time interval of the study, the Eastern Mediterranean was a warm subtropical area with fluctuating influxes of terrestrial organic matter. The global warm MIS 21 initiation, the sea-level drop in MIS 20, and high productivity accompanied by enhanced organic matter burial during MIS 19 are the most notable environmental changes evidenced in the study area at this time. All the studied fossil groups seem to have been affected by the warming that took place during the early part of MIS 21, with increases in biomass observed for the invertebrate groups (foraminifera, ostracods and sponges) and a reduction in DVM for mesopelagic fishes. Similarly, large variabilities in foraminifera, ostracod and sponge biomasses are observed within the MIS 19 interglacial. However, we could not find evidence of a disruption in the fish DVM pattern in this interval, although the fish abundances and body sizes have been shown to be affected by this interglacial (Agiadi et al., 2023). Planktonic foraminifera biomass was negatively affected by the MIS 20 and MIS 18 glacials. Although our ecosystem-level approach is challenging, it offers a holistic approach for assessing the impacts of paleoenvironmental changes that can be most informative for ecosystem management.

**Acknowledgements**

This research was funded by the Austrian Science Fund (FWF) Grant DOI 10.55776/M2894 (P.I.: KA). For the purpose of open access, the author has applied a CC BY public copyright license to any Author Accepted Manuscript version arising from this submission. FQ was supported by the National programs Tellus-INTERRVIE of CNRS-INSU. AFA and JMT received funding from the Spanish project ProOceans (Ministerio de Ciencia e Innovación, Proyectos de I + D + I (RETOSPID2020-118097RB-I00)). The authors acknowledge institutional support of the 'Severo Ochoa Center of Excellence' accreditation (CEX2019-000928-S) and the Catalan government through the iMARES research group of quality at ICM-CSIC. We warmly thank Arnauld Vinçon-Laugier for technical assistance with the mass spectrometer, Uli Treffert for assistance in the SBiK-F laboratories, Jean-Jacques Cornée and Pierre Moissette for showing us the Lardos section, and George Kontakiotis and Vasiliki Lianou for their help in the field.

**Authors Contribution**

Conceptualization: KA, FQ; Formal analysis: KA, IV, AV, AFA, JMT, FQ; Funding acquisition: KA, FQ; Investigation: KA, IV, AV, EK, SZ, AFA, JMT, FQ; Methodology: KA, IV, SZ, AFA, JMT, FQ; Supervision: KA, FQ; Writing – original draft: KA, IV, AV, SZ, AFA, JMT, FQ; Writing – review and editing: EK.

**Data and Code Availability Statement**

The data produced for this work is publicly available in (Agiadi et al., 2024b). The code to estimate the fish lifetime-average depth is publicly available in (Fuster-Alonso et al., 2024).

**References**

Agiadi, K., Triantaphyllou, M., Girone, A., Karakitsios, V., and Dermitzakis, M.: Paleobathymetric interpretation of the fish otoliths from the lower - middle Quaternary deposits of Kephallonia and Zakynthos islands (Ionian Sea, Western Greece), Rivista Italiana di Paleontologia e Stratigrafia, 116, 63–78, https://doi.org/10.13130/2039-4942/5941, 2010.

Agiadi, K., Triantaphyllou, M., Girone, A., and Karakitsios, V.: The early Quaternary palaeobiogeography of the eastern Ionian deep-sea Teleost fauna: A novel palaeocirculation approach, Palaeogeography, Palaeoclimatology, Palaeoecology, 306, 228–242, https://doi.org/10.1016/j.palaeo.2011.04.029, 2011.

Agiadi, K., Girone, A., Koskeridou, E., Moissette, P., Cornée, J.-J., and Quillévéré, F.: Pleistocene marine fish invasions and paleoenvironmental reconstructions in the eastern Mediterranean, Quaternary Science Reviews, 196, 80–99, https://doi.org/10.1016/j.quascirev.2018.07.037, 2018.

Agiadi, K., Azzarone, M., Hua, Q., Kaufman, D. S., Thivaiou, D., and Albano, P. G.: The taphonomic clock in fish otoliths, Paleobiology, 48, 154–170, https://doi.org/10.1017/pab.2021.30, 2022.

Agiadi, K., Quillévéré, F., Nawrot, R., Sommeville, T., Coll, M., Koskeridou, E., Fietzke, J., and Zuschin, M.: Palaeontological evidence for community-level decrease in mesopelagic fish size during Pleistocene climate warming in the eastern Mediterranean, Proceedings of the Royal Society B: Biological Sciences, 290, 20221994, https://doi.org/10.1098/rspb.2022.1994, 2023.

Agiadi, K., Vasiliev, I., Butiseacă, G., Kontakiotis, G., Thivaiou, D., Besiou, E., Zarkogiannis, S., Koskeridou, E., Antonarakou, A., and Mulch, A.: Coupled otolith and foraminifera oxygen and carbon stable isotopes evidence paleoceanographic changes and fish metabolic responses, Biogeosciences, 21, 3869–3881, https://doi.org/10.5194/bg-21-3869-2024, 2024a.

Agiadi, K., Vasiliev, I., Vite, A., Zarkogiannis, S. D., and Quillévéré, F.: Dataset for Agiadi et al 2024 "Pelagic ecosystem responses to changes in seawater conditions during the Middle Pleistocene Transition in the Eastern Mediterranean," https://doi.org/10.5281/zenodo.14623783, 2024b.

Aksnes, D. L., Løtvedt, A. S., Lindemann, C., Calleja, M. L., Morán, X. A. G., Kaarvedt, S., and Thingstad, T. F.: Effects of migrating mesopelagic fishes on the biological carbon pump, Marine Ecology Progress Series, 717, 107–126, https://doi.org/10.3354/meps14373, 2023.

Alvarez, B., Frings, P. J., Clymans, W., Fontorbe, G., and Conley, D. J.: Assessing the Potential of Sponges (Porifera) as Indicators of Ocean Dissolved Si Concentrations, Front. Mar. Sci., 4, https://doi.org/10.3389/fmars.2017.00373, 2017.

An, Z., Zhou, W., Zhang, Z., Zhang, X., Liu, Z., Sun, Y., Clemens, S. C., Wu, L., Zhao, J., Shi, Z., Ma, X., Yan, H., Li, G., Cai, Y., Yu, J., Sun, Y., Li, S., Zhang, Y., Stepanek, C., Lohmann, G., Dong, G., Cheng, H., Liu, Y., Jin, Z., Li, T., Hao, Y., Lei, J., and Cai, W.: Mid-Pleistocene climate transition triggered by Antarctic Ice Sheet growth, Science, 385, 560–565, https://doi.org/10.1126/science.abn4861, 2024.

Antonarakou, A., Kontakiotis, G., Vasilatos, C., Besiou, E., Zarkogiannis, S., Drinia, H., Mortyn, P. G., Tsaparas, N., Makri, P., and Karakitsios, V.: Evaluating the Effect of Marine Diagenesis on Late Miocene Pre-Evaporitic Sedimentary Successions of Eastern Mediterranean Sea, IOP Conf. Ser.: Earth Environ. Sci., 221, 012051, https://doi.org/10.1088/1755-1315/221/1/012051, 2019.

Ao, H., Rohling, E. J., Li, X., Song, Y., Roberts, A. P., Han, Y., Poulsen, C. J., Jonell, T. N., Liebrand, D., Sun, Q., Li, X., Qiang, X., Zhang, P., and Dekkers, M. J.: Northern hemisphere ice sheet expansion intensified Asian aridification and the winter monsoon across the mid-Pleistocene transition, Commun Earth Environ, 4, 1–11, https://doi.org/10.1038/s43247-023-00686-9, 2023.

Auer, G., Petrick, B., Yoshimura, T., Mamo, B. L., Reuning, L., Takayanagi, H., De Vleeschouwer, D., and Martinez-Garcia, A.: Intensified organic carbon burial on the Australian shelf after the Middle Pleistocene transition, Quaternary Science Reviews, 262, 106965, https://doi.org/10.1016/j.quascirev.2021.106965, 2021.

Aumont, O., Maury, O., Lefort, S., and Bopp, L.: Evaluating the Potential Impacts of the Diurnal Vertical Migration by Marine Organisms on Marine Biogeochemistry, Global Biogeochemical Cycles, 32, 1622–1643, https://doi.org/10.1029/2018GB005886, 2018.

Badcock, J. and Merrett, N. R.: Midwater fishes in the eastern North Atlantic—I. Vertical distribution and associated biology in 30°N, 23°W, with developmental notes on certain myctophids, Progress in Oceanography, 7, 3–58, https://doi.org/10.1016/0079-6611(76)90003-3, 1976.

Berends, C. J., Köhler, P., Lourens, L. J., and van de Wal, R. S. W.: On the Cause of the Mid-Pleistocene Transition, Reviews of Geophysics, 59, e2020RG000727, https://doi.org/10.1029/2020RG000727, 2021.

Besiou, E., Vasiliev, I., Kontakiotis, G., Agiadi, K., Methner, K., Mulch, A., Krijgsman, W., and Antonarakou, A.: Large and rapid salinity fluctuations affected the eastern Mediterranean at the Tortonian–Messinian transition, Palaeogeography, Palaeoclimatology, Palaeoecology, 656, 112568, https://doi.org/10.1016/j.palaeo.2024.112568, 2024.

Boscolo-Galazzo, F., Crichton, K. A., Ridgwell, A., Mawbey, E. M., Wade, B. S., and Pearson, P. N.: Temperature controls carbon cycling and biological evolution in the ocean twilight zone, Science, 371, 1148–1152, https://doi.org/10.1126/science.abb6643, 2021.

Brierley, A. S.: Diel vertical migration, Current Biology, 24, R1074–R1076, https://doi.org/10.1016/j.cub.2014.08.054, 2014.

Campana, S. E.: Chemistry and composition of fish otoliths: pathways, mechanisms and applications, Mar Ecol Progr Ser, 188, 263–297, 1999.

Chung, M.-T., Trueman, C. N., Godiksen, J. A., Holmstrup, M. E., and Grønkjær, P.: Field metabolic rates of teleost fishes are recorded in otolith carbonate, Commun Biol, 2, 1–10, https://doi.org/10.1038/s42003-018-0266-5, 2019a.

Chung, M.-T., Trueman, C. N., Godiksen, J. A., Grønkjær, P., Chung, M.-T., Trueman, C. N., Godiksen, J. A., and Grønkjær, P.: Otolith δ13C values as a metabolic proxy: approaches and mechanical underpinnings, Mar. Freshwater Res., 70, 1747–1756, https://doi.org/10.1071/MF18317, 2019b.

Cirilli, O., Saarinen, J., Bukhsianidze, M., Lordkipanidze, D., and Bernor, R. L.: *Equus suessenbornensis* from Akhalkalaki (Georgia, Caucasus): a review with new insights on the paleoecology, paleobiogeography and evolution of the palearctic large-sized equids during the Early – Middle Pleistocene Transition, Quaternary Science Reviews, 314, 108188, https://doi.org/10.1016/j.quascirev.2023.108188, 2023.

Clark, P. U., Archer, D., Pollard, D., Blum, J. D., Rial, J. A., Brovkin, V., Mix, A. C., Pisias, N. G., and Roy, M.: The middle Pleistocene transition: characteristics, mechanisms, and implications for long-term changes in atmospheric pCO2, Quaternary Science Reviews, 25, 3150–3184, https://doi.org/10.1016/j.quascirev.2006.07.008, 2006.

Cornée, J.-J., Moissette, P., Joannin, S., Suc, J.-P., Quillévéré, F., Krijgsman, W., Hilgen, F., Koskeridou, E., Münch, P., Lécuyer, C., and Desvignes, P.: Tectonic and climatic controls on coastal sedimentation: The Late Pliocene–Middle Pleistocene of northeastern Rhodes, Greece, Sedimentary Geology, 187, 159–181, https://doi.org/10.1016/j.sedgeo.2005.12.026, 2006.

Cornée, J.-J., Quillévéré, F., Moissette, P., Fietzke, J., López-Otálvaro, G. E., Melinte-Dobrinescu, M., Philippon, M., Hinsbergen, D. J. J. van, Agiadi, K., Koskeridou, E., and Münch, P.: Tectonic motion in oblique subduction forearcs: insights from the revisited Middle and Upper Pleistocene deposits of Rhodes, Greece, Journal of the Geological Society, 176, 78–96, https://doi.org/10.1144/jgs2018-090, 2019.

DeNinno, L. H., Cronin, T. M., Rodriguez-Lazaro, J., and Brenner, A.: An early to mid-Pleistocene deep Arctic Ocean ostracode fauna with North Atlantic affinities, Palaeogeography, Palaeoclimatology, Palaeoecology, 419, 90–99, https://doi.org/10.1016/j.palaeo.2014.07.026, 2015.

Diester-Haass, L., Billups, K., and Lear, C.: Productivity changes across the mid-Pleistocene climate transition, Earth-Science Reviews, 179, 372–391, https://doi.org/10.1016/j.earscirev.2018.02.016, 2018.

Dufour, E., Cappetta, H., Denis, A., Dauphin, Y., and Mariotti, A.: Otolith diagenesis comparing microstructural, mineralogical and geochemical data: Application to Pliocene fossils from southeastern France [La diagenese des otolithes

par la comparaison des donnees microstructurales, mineralogiques et geochimiques: Application aux fossiles du Pliocene du Sud-Est de la France], Bulletin de la Societe Geologique de France, 171, 521–532, 2000.

Eduardo, L. N., Bertrand, A., Mincarone, M. M., Martins, J. R., Frédou, T., Assunção, R. V., Lima, R. S., Ménard, F., Le Loc'h, F., and Lucena-Frédou, F.: Distribution, vertical migration, and trophic ecology of lanternfishes (Myctophidae) in the Southwestern Tropical Atlantic, Progress in Oceanography, 199, 102695, https://doi.org/10.1016/j.pocean.2021.102695, 2021.

Eichner, D., Schmiedl, G., Titschack, J., Ferreira, M., Triantaphyllou, M., Andersen, N., and Milker, Y.: Humid climate phases on the Island of Rhodes (Greece) during the late Pliocene at times of sapropel formation, Marine Micropaleontology, 187, 102341, https://doi.org/10.1016/j.marmicro.2024.102341, 2024.

El Frihmat, Y., Hebbeln, D., Jaaidi, E. B., and Mhammdi, N.: Reconstruction of productivity signal and deep-water conditions in Moroccan Atlantic margin (~35°N) from the last glacial to the Holocene, Springerplus, 4, https://doi.org/10.1186/s40064-015-0853-6, 2015.

Elderfield, H., Ferretti, P., Greaves, M., Crowhurst, S., McCave, I. N., Hodell, D., and Piotrowski, A. M.: Evolution of Ocean Temperature and Ice Volume Through the Mid-Pleistocene Climate Transition, Science, 337, 704–709, https://doi.org/10.1126/science.1221294, 2012.

Fairbanks, R. G. and Matthews, R. K.: The marine oxygen isotope record in Pleistocene coral, Barbados, West Indies, Quaternary Research, 10, 181–196, https://doi.org/10.1016/0033-5894(78)90100-X, 1978.

Fuster-Alonso, A., Mestre Tomás, J., and Agiadi, K.: Code for estimating the fish lifetime-average depth for Agiadi et al_2024 "Pelagic ecosystem responses to changes in seawater conditions during the Middle Pleistocene Transition in the Eastern Mediterranean," 2024.

Gallo, N. D. and Levin, L. A.: Chapter Three - Fish Ecology and Evolution in the World's Oxygen Minimum Zones and Implications of Ocean Deoxygenation, in: Advances in Marine Biology, vol. 74, edited by: Curry, B. E., Academic Press, 117–198, https://doi.org/10.1016/bs.amb.2016.04.001, 2016.

Gibson, T. G.: Planktonic benthonic foraminiferal ratios: Modern patterns and Tertiary applicability, Marine Micropaleontology, 15, 29–52, https://doi.org/10.1016/0377-8398(89)90003-0, 1989.

Girone, A. and Varola, A.: Fish otoliths from the middle Pleistocene deposits of Montalbano Jonico (Southern Italy), Bollettino della Societa Paleontologica Italiana, 40, 431–443, 2001.

Girone, A., Nolf, D., and Cappetta, H.: Pleistocene fish otoliths from the Mediterranean Basin: a synthesis, Geobios, 39, 651–671, https://doi.org/10.1016/j.geobios.2005.05.004, 2006.

Girone, A., De Astis, A., Sierro, F. J., Hernández-Almeida, I., Garcia, M. A., Sánchez Goñi, M. F., Maiorano, P., Marino, M., Trotta, S., and Hodell, D.: Planktonic foraminifera response to orbital and millennial-scale climate variability at the southern Iberian Margin (IODP Site U1385) during Marine Isotope Stages 20 and 19, Palaeogeography, Palaeoclimatology, Palaeoecology, 615, 111450, https://doi.org/10.1016/j.palaeo.2023.111450, 2023.

Gooday, A. J. and Jorissen, F. J.: Benthic Foraminiferal Biogeography: Controls on Global Distribution Patterns in Deep-Water Settings, Annual Review of Marine Science, 4, 237–262, https://doi.org/10.1146/annurev-marine-120709-142737, 2012.

Goren, M. and Galil, B. S.: A checklist of the deep sea fishes of the Levant Sea, Mediterranean Sea, Zootaxa, 3994, 507–530, https://doi.org/10.11646/zootaxa.3994.4.2, 2015.

Grigoratou, M., Monteiro, F. M., Schmidt, D. N., Wilson, J. D., Ward, B. A., and Ridgwell, A.: A trait-based modelling approach to planktonic foraminifera ecology, Biogeosciences, 16, 1469–1492, https://doi.org/10.5194/bg-16-1469-2019, 2019.

Grigoratou, M., Monteiro, F. M., Wilson, J. D., Ridgwell, A., and Schmidt, D. N.: Exploring the impact of climate change on the global distribution of non-spinose planktonic foraminifera using a trait-based ecosystem model, Global Change Biology, 28, 1063–1076, https://doi.org/10.1111/gcb.15964, 2022.

Head, M. J. and Gibbard, P. L.: Early–Middle Pleistocene transitions: Linking terrestrial and marine realms, Quaternary International, 389, 7–46, https://doi.org/10.1016/j.quaint.2015.09.042, 2015.

Hopmans, E. C., Weijers, J. W. H., Schefuß, E., Herfort, L., Sinninghe Damsté, J. S., and Schouten, S.: A novel proxy for terrestrial organic matter in sediments based on branched and isoprenoid tetraether lipids, Earth and Planetary Science Letters, 224, 107–116, https://doi.org/10.1016/j.epsl.2004.05.012, 2004.

Hu, W., Hao, Z., Du, P., Di Vincenzo, F., Manzi, G., Cui, J., Fu, Y.-X., Pan, Y.-H., and Li, H.: Genomic inference of a severe human bottleneck during the Early to Middle Pleistocene transition, Science, 381, 979–984, https://doi.org/10.1126/science.abq7487, 2023.

Huang, H.-H. M., Yasuhara, M., Iwatani, H., Yamaguchi, T., Yamada, K., and Mamo, B.: Deep-sea ostracod faunal dynamics in a marginal sea: Biotic response to oxygen variability and mid-Pleistocene global changes, Paleobiology, 45, 85–97, https://doi.org/10.1017/pab.2018.37, 2019.

Incarbona, A., Marino, G., Di Stefano, E., Grelaud, M., Pelosi, N., Rodriguez-Sanz, L., and Rohling, E. J.: Middle-Late Pleistocene Eastern Mediterranean nutricline depth and coccolith preservation linked to Monsoon activity and Atlantic Meridional Overturning Circulation, Global And Planetary Change, 217, https://doi.org/10.1016/j.gloplacha.2022.103946, 2022.

Jing, Y., Zhang, T., Zhu, B., Zhao, J., Zhao, X., Dou, Y., Li, Q., Cai, F., Hu, B., and Dong, L.: Organic carbon burial and their implication on sea surface primary productivity in the middle Okinawa Trough over the past 200 ka, Front. Mar. Sci., 11, https://doi.org/10.3389/fmars.2024.1331940, 2024.

Jorissen, F. J., de Stigter, H. C., and Widmark, J. G. V.: A conceptual model explaining benthic foraminiferal microhabitats, Marine Micropaleontology, 26, 3–15, https://doi.org/10.1016/0377-8398(95)00047-X, 1995.

Kalish, J. M.: 13C and 18O isotopic disequilibria in fish otoliths: metabolic and kinetic effects, Mar Ecol Progr Ser, 75, 191–203, 1991a.

Kalish, J. M.: Oxygen and carbon stable isotopes in the otoliths of wild and laboratory-reared Australian salmon ( Arripis trutta ), Mar. Biol., 110, 37–47, https://doi.org/10.1007/BF01313090, 1991b.

Killen, S. S., Atkinson, D., and Glazier, D. S.: The intraspecific scaling of metabolic rate with body mass in fishes depends on lifestyle and temperature, Ecology Letters, 13, 184–193, https://doi.org/10.1111/j.1461-0248.2009.01415.x, 2010.

Kim, J., Meer, J. V. D., Schouten, S., Helmke, P., Willmott, V., Sangiorgi, F., Koç, N., Hopmans, E., and Damsté, J. S.: New indices and calibrations derived from the distribution of crenarchaeal isoprenoid tetraether lipids: Implications for past sea surface temperature reconstructions, https://doi.org/10.1016/J.GCA.2010.05.027, 2010.

Kim, J.-H., Schouten, S., Rodrigo-Gámiz, M., Rampen, S., Marino, G., Huguet, C., Helmke, P., Buscail, R., Hopmans, E. C., Pross, J., Sangiorgi, F., Middelburg, J. B. M., and Sinninghe Damsté, J. S.: Influence of deep-water derived isoprenoid tetraether lipids on the TEX86H paleothermometer in the Mediterranean Sea, Geochimica et Cosmochimica Acta, 150, 125–141, https://doi.org/10.1016/j.gca.2014.11.017, 2015.

Kinzer, J. and Schulz, K.: Vertical distribution and feeding patterns of midwater fish in the central equatorial Atlantic, Marine Biology, 85, 313–322, https://doi.org/10.1007/BF00393252, 1985.

Konijnendijk, T. Y. M., Ziegler, M., and Lourens, L. J.: On the timing and forcing mechanisms of late Pleistocene glacial terminations: Insights from a new high-resolution benthic stable oxygen isotope record of the eastern Mediterranean, Quaternary Science Reviews, 129, 308–320, https://doi.org/10.1016/j.quascirev.2015.10.005, 2015.

Kontakiotis, G., Butiseacă, G. A., Antonarakou, A., Agiadi, K., Zarkogiannis, S. D., Krsnik, E., Besiou, E., Zachariasse, W. J., Lourens, L., Thivaiou, D., Koskeridou, E., Moissette, P., Mulch, A., Karakitsios, V., and Vasiliev, I.: Hypersalinity accompanies tectonic restriction in the eastern Mediterranean prior to the Messinian Salinity Crisis, Palaeogeography, Palaeoclimatology, Palaeoecology, 592, 110903, https://doi.org/10.1016/j.palaeo.2022.110903, 2022.

Lanzante, J. R.: Resistant, Robust and Non-Parametric Techniques for the Analysis of Climate Data: Theory and Examples, Including Applications to Historical Radiosonde Station Data, International Journal of Climatology, 16, 1197–1226, https://doi.org/10.1002/(SICI)1097-0088(199611)16:11<1197::AID-JOC89>3.0.CO;2-L, 1996.

Lea, D. W., Martin, P. A., Pak, D. K., and Spero, H. J.: Reconstructing a 350 ky history of sea level using planktonic Mg/Ca and oxygen isotope records from a Cocos Ridge core, Quaternary Science Reviews, 21, 283–293, https://doi.org/10.1016/S0277-3791(01)00081-6, 2002.

Lindmark, M., Ohlberger, J., and Gårdmark, A.: Optimum growth temperature declines with body size within fish species, Global Change Biology, 28, 2259–2271, https://doi.org/10.1111/gcb.16067, 2022.

Lisiecki, L. E. and Raymo, M. E.: A Pliocene-Pleistocene stack of 57 globally distributed benthic δ18O records, Paleoceanography, 20, PA1003, https://doi.org/10.1029/2004PA001071, 2005.

Łukowiak, M.: Utilizing sponge spicules in taxonomic, ecological and environmental reconstructions: a review, PeerJ, 8, e10601, https://doi.org/10.7717/peerj.10601, 2020.

Margari, V., Hodell, D. A., Parfitt, S. A., Ashton, N. M., Grimalt, J. O., Kim, H., Yun, K.-S., Gibbard, P. L., Stringer, C. B., Timmermann, A., and Tzedakis, P. C.: Extreme glacial cooling likely led to hominin depopulation of Europe in the Early Pleistocene, Science, 381, 693–699, https://doi.org/10.1126/science.adf4445, 2023.

Marino, M., Maiorano, P., and Lirer, F.: Changes in calcareous nannofossil assemblages during the Mid-Pleistocene Revolution, Marine Micropaleontology, 69, 70–90, https://doi.org/10.1016/j.marmicro.2007.11.010, 2008.

Marino, M., Girone, A., Gallicchio, S., Herbert, T., Addante, M., Bazzicalupo, P., Quivelli, O., Bassinot, F., Bertini, A., Nomade, S., Ciaranfi, N., and Maiorano, P.: Climate variability during MIS 20–18 as recorded by alkenone-SST and calcareous plankton in the Ionian Basin (central Mediterranean), Palaeogeography, Palaeoclimatology, Palaeoecology, 560, 110027, https://doi.org/10.1016/j.palaeo.2020.110027, 2020.

Marino, M., Rodrigues, T., Quivelli, O., Girone, A., Maiorano, P., and Bassinot, F.: Paleoproductivity proxies and alkenone precursors in the Western Mediterranean during the Early-Middle Pleistocene transition, Palaeogeography, Palaeoclimatology, Palaeoecology, 601, 111104, https://doi.org/10.1016/j.palaeo.2022.111104, 2022.

Martínez-Dios, A., Pelejero, C., Cobacho, S., Movilla, J., Dinarès-Turell, J., and Calvo, E.: A 1-Million-Year Record of Environmental Change in the Central Mediterranean Sea From Organic Molecular Proxies, Paleoceanography and Paleoclimatology, 36, e2021PA004289, https://doi.org/10.1029/2021PA004289, 2021.

Martino, J. C., Doubleday, Z. A., Chung, M.-T., and Gillanders, B. M.: Experimental support towards a metabolic proxy in fish using otolith carbon isotopes, Journal of Experimental Biology, 223, https://doi.org/10.1242/jeb.217091, 2020.

Milker, Y., Weinkauf, M. F. G., Titschack, J., Freiwald, A., Krüger, S., Jorissen, F. J., and Schmiedl, G.: Testing the applicability of a benthic foraminiferal-based transfer function for the reconstruction of paleowater depth changes in Rhodes (Greece) during the early Pleistocene, PLOS ONE, 12, e0188447, https://doi.org/10.1371/journal.pone.0188447, 2017.

Milker, Y., Jorissen, F. J., Riller, U., Reicherter, K., Titschack, J., Weinkauf, M. F. G., Theodor, M., and Schmiedl, G.: Paleo-ecologic and neotectonic evolution of a marine depositional environment in SE Rhodes (Greece) during the early Pleistocene, Quaternary Science Reviews, 213, 120–132, https://doi.org/10.1016/j.quascirev.2019.04.021, 2019.

Minnett, P. J., Alvera-Azcárate, A., Chin, T. M., Corlett, G. K., Gentemann, C. L., Karagali, I., Li, X., Marsouin, A., Marullo, S., Maturi, E., Santoleri, R., Saux Picart, S., Steele, M., and Vazquez-Cuervo, J.: Half a century of satellite remote sensing of sea-surface temperature, Remote Sensing of Environment, 233, 111366, https://doi.org/10.1016/j.rse.2019.111366, 2019.

Movellan, A., Schiebel, R., Zubkov, M. V., Smyth, A., and Howa, H.: Protein biomass quantification of unbroken individual foraminifers using nano-spectrophotometry, Biogeosciences, 9, 3613–3623, https://doi.org/10.5194/bg-9-3613-2012, 2012.

Mytilineou, C., Politou, C. Y., Papaconstantinou, C., Kavadas, S., D'Onghia, G., and Sion, L.: Deep-water fish fauna in the Eastern Ionian Sea, Belg J Zool, 135, 229–233, 2005.

Nomade, S., Bassinot, F., Marino, M., Simon, Q., Dewilde, F., Maiorano, P., Isguder, G., Blamart, D., Girone, A., Scao, V., Pereira, A., Toti, F., Bertini, A., Combourieu-Nebout, N., Peral, M., Bourlès, D. L., Petrosino, P., Gallicchio, S., and Ciaranfi, N.: High-resolution foraminifer stable isotope record of MIS 19 at Montalbano Jonico, southern Italy: A window into Mediterranean climatic variability during a low-eccentricity interglacial, Quaternary Science Reviews, 205, 106–125, https://doi.org/10.1016/j.quascirev.2018.12.008, 2019.

Olivar, M. P., Bernal, A., Molí, B., Peña, M., Balbín, R., Castellón, A., Miquel, J., and Massutí, E.: Vertical distribution, diversity and assemblages of mesopelagic fishes in the western Mediterranean, Deep Sea Research Part I: Oceanographic Research Papers, 62, 53–69, https://doi.org/10.1016/j.dsr.2011.12.014, 2012.

Olivar, M. P., Hulley, P. A., Castellón, A., Emelianov, M., López, C., Tuset, V. M., Contreras, T., and Molí, B.: Mesopelagic fishes across the tropical and equatorial Atlantic: Biogeographical and vertical patterns, Progress in Oceanography, 151, 116–137, https://doi.org/10.1016/j.pocean.2016.12.001, 2017.

Olivar, M. P., Contreras, T., Hulley, P. A., Emelianov, M., López-Pérez, C., Tuset, V., and Castellón, A.: Variation in the diel vertical distributions of larvae and transforming stages of oceanic fishes across the tropical and equatorial Atlantic, Progress in Oceanography, 160, 83–100, https://doi.org/10.1016/j.pocean.2017.12.005, 2018.

Peeters, F. J. C., Brummer, G.-J. A., and Ganssen, G.: The effect of upwelling on the distribution and stable isotope composition of *Globigerina bulloides* and *Globigerinoides ruber* (planktic foraminifera) in modern surface waters of the NW Arabian Sea, Global and Planetary Change, 34, 269–291, https://doi.org/10.1016/S0921-8181(02)00120-0, 2002.

Peral, M., Blamart, D., Bassinot, F., Daëron, M., Dewilde, F., Rebaubier, H., Nomade, S., Girone, A., Marino, M., Maiorano, P., and Ciaranfi, N.: Changes in temperature and oxygen isotopic composition of Mediterranean water during the Mid-

Pleistocene transition in the Montalbano Jonico section (southern Italy) using the clumped-isotope thermometer, Palaeogeography, Palaeoclimatology, Palaeoecology, 544, 109603, https://doi.org/10.1016/j.palaeo.2020.109603, 2020.

Perry, A. L., Low, P. J., Ellis, J. R., and Reynolds, J. D.: Climate Change and Distribution Shifts in Marine Fishes, Science, 308, 1912–1915, https://doi.org/10.1126/science.1111322, 2005.

Pinti, J., DeVries, T., Norin, T., Serra-Pompei, C., Proud, R., Siegel, D. A., Kiørboe, T., Petrik, C. M., Andersen, K. H., Brierley, A. S., and Visser, A. W.: Model estimates of metazoans' contributions to the biological carbon pump, Biogeosciences, 20, 997–1009, https://doi.org/10.5194/bg-20-997-2023, 2023.

Porz, A., Zuschin, M., Strotz, L., Koskeridou, E., Simoens, K., Lukić, R., Thivaiou, D., Quillévéré, F., and Agiadi, K.: Controls on long-term changes in bathyal bivalve biomass: The Pleistocene glacial–interglacial record in the eastern Mediterranean, Deep Sea Research Part I: Oceanographic Research Papers, 104224, https://doi.org/10.1016/j.dsr.2023.104224, 2024.

Pracht, H., Metcalfe, B., and Peeters, F. J. C.: Oxygen isotope composition of the final chamber of planktic foraminifera provides evidence of vertical migration and depth-integrated growth, Biogeosciences, 16, 643–661, https://doi.org/10.5194/bg-16-643-2019, 2019.

Quillévéré, F., Cornée, J.-J., Moissette, P., López-Otálvaro, G. E., van Baak, C., Münch, P., Melinte-Dobrinescu, M. C., and Krijgsman, W.: Chronostratigraphy of uplifted Quaternary hemipelagic deposits from the Dodecanese island of Rhodes (Greece), Quaternary Research, 86, 79–94, https://doi.org/10.1016/j.yqres.2016.05.002, 2016.

Quillévéré, F., Nouailhat, N., Joannin, S., Cornée, J.-J., Moissette, P., Lécuyer, C., Fourel, F., Agiadi, K., Koskeridou, E., and Escarguel, G.: An onshore bathyal record of tectonics and climate cycles at the onset of the Early-Middle Pleistocene Transition in the eastern Mediterranean, Quaternary Science Reviews, 209, 23–39, https://doi.org/10.1016/j.quascirev.2019.02.012, 2019.

Quivelli, O., Marino, M., Rodrigues, T., Girone, A., Maiorano, P., Abrantes, F., Salgueiro, E., and Bassinot, F.: Surface and deep water variability in the Western Mediterranean (ODP Site 975) during insolation cycle 74: High-resolution calcareous plankton and molecular biomarker signals, Palaeogeography, Palaeoclimatology, Palaeoecology, 542, 109583, https://doi.org/10.1016/j.palaeo.2019.109583, 2020.

Quivelli, O., Marino, M., Rodrigues, T., Girone, A., Maiorano, P., Bertini, A., Niccolini, G., Trotta, S., and Bassinot, F.: Multiproxy record of suborbital-scale climate changes in the Algero-Balearic Basin during late MIS 20 - Termination IX, Quaternary Science Reviews, 260, 106916, https://doi.org/10.1016/j.quascirev.2021.106916, 2021.

R Development Core Team: R: A language and environment for statistical computing, 2024.

Ravelo, A. C. and Hillaire-Marcel, C.: The use of oxygen and carbon isotopes of foraminifera in Paleoceanography, in: C. Hillaire-Marcel, A. de Vernal, Proxies in Late Cenozoic Paleoceanography, Elsevier, Amsterdam, 735–764, 2007.

Rodionov, S. N.: A sequential algorithm for testing climate regime shifts, Geophysical Research Letters, 31, https://doi.org/10.1029/2004GL019448, 2004.

Rodrigues, T., Alonso-García, M., Hodell, D. A., Rufino, M., Naughton, F., Grimalt, J. O., Voelker, A. H. L., and Abrantes, F.: A 1-Ma record of sea surface temperature and extreme cooling events in the North Atlantic: A perspective from the Iberian Margin, Quaternary Science Reviews, 172, 118–130, https://doi.org/10.1016/j.quascirev.2017.07.004, 2017.

Rohling, E., Sprovieri, M., Cane, T., Casford, J., Cooke, S., Bouloubassi, I., Emeis, K., Schiebel, R., Rogerson, M., Hayes, A., Jorissen, F., and Kroon, D.: Reconstructing past planktic foraminiferal habitats using stable isotope data: a case history for Mediterranean sapropel S5, Marine Micropaleontology, 50, 89–123, https://doi.org/10.1016/S0377-8398(03)00068-9, 2004.

Room, A., Franco-Gaviria, F., and Urrego, D.: rshift: paleoecology and regime shift analysis, 2020.

Rossi, V., Azzarone, M., Capraro, L., Faranda, C., Ferretti, P., Macrì, P., and Scarponi, D.: Dynamics of benthic marine communities across the Early-Middle Pleistocene boundary in the Mediterranean region (Valle di Manche, Southern Italy): Biotic and stratigraphic implications, Palaeogeography, Palaeoclimatology, Palaeoecology, 495, 127–138, https://doi.org/10.1016/j.palaeo.2017.12.042, 2018.

Rountrey, A. N., Coulson, P. G., Meeuwig, J. J., and Meekan, M.: Water temperature and fish growth: otoliths predict growth patterns of a marine fish in a changing climate, Global Change Biology, 20, 2450–2458, https://doi.org/10.1111/gcb.12617, 2014.

Rühlemann, C., Frank, M., Hale, W., Mangini, A., Mulitza, S., Müller, P. J., and Wefer, G.: Late Quaternary productivity changes in the western equatorial Atlantic: Evidence from 230Th-normalized carbonate and organic carbon accumulation rates, Marine Geology, 135, 127–152, https://doi.org/10.1016/S0025-3227(96)00048-5, 1996.

Sánchez Goñi, M. F., Extier, T., Polanco-Martínez, J. M., Zorzi, C., Rodrigues, T., and Bahr, A.: Moist and warm conditions in Eurasia during the last glacial of the Middle Pleistocene Transition, Nat Commun, 14, 2700, https://doi.org/10.1038/s41467-023-38337-4, 2023.

Schiebel, R.: Planktic foraminiferal sedimentation and the marine calcite budget, Global Biogeochemical Cycles, 16, 3-1-3–21, https://doi.org/10.1029/2001GB001459, 2002.

Schiebel, R. and Hemleben, C.: Planktic Foraminifers in the Modern Ocean, Springer, Berlin, Heidelberg, https://doi.org/10.1007/978-3-662-50297-6, 2017.

Schiebel, R. and Movellan, A.: First-order estimate of the planktic foraminifer biomass in the modern ocean, Earth System Science Data, 4, 75–89, https://doi.org/10.5194/essd-4-75-2012, 2012.

Schiebel, R., Smart, S. M., Jentzen, A., Jonkers, L., Morard, R., Meilland, J., Michel, E., Coxall, H. K., Hull, P. M., de Garidel-Thoron, T., Aze, T., Quillévéré, F., Ren, H., Sigman, D. M., Vonhof, H. B., Martínez-García, A., Kučera, M., Bijma, J., Spero, H. J., and Haug, G. H.: Advances in planktonic foraminifer research: New perspectives for paleoceanography, Revue de Micropaléontologie, 61, 113–138, https://doi.org/10.1016/j.revmic.2018.10.001, 2018.

Schmidt, D. N., Renaud, S., Bollmann, J., Schiebel, R., and Thierstein, H. R.: Size distribution of Holocene planktic foraminifer assemblages: biogeography, ecology and adaptation, Marine Micropaleontology, 50, 319–338, https://doi.org/10.1016/S0377-8398(03)00098-7, 2004.

Schouten, S., Hopmans, E. C., Schefuß, E., and Sinninghe Damsté, J. S.: Distributional variations in marine crenarchaeotal membrane lipids: a new tool for reconstructing ancient sea water temperatures?, Earth and Planetary Science Letters, 204, 265–274, https://doi.org/10.1016/S0012-821X(02)00979-2, 2002.

Schouten, S., Hopmans, E. C., Rosell-Melé, A., Pearson, A., Adam, P., Bauersachs, T., Bard, E., Bernasconi, S. M., Bianchi, T. S., Brocks, J. J., Carlson, L. T., Castañeda, I. S., Derenne, S., Selver, A. D., Dutta, K., Eglinton, T., Fosse, C., Galy, V., Grice, K., Hinrichs, K.-U., Huang, Y., Huguet, A., Huguet, C., Hurley, S., Ingalls, A., Jia, G., Keely, B., Knappy, C., Kondo, M., Krishnan, S., Lincoln, S., Lipp, J., Mangelsdorf, K., Martínez-García, A., Ménot, G., Mets, A., Mollenhauer, G.,

Ohkouchi, N., Ossebaar, J., Pagani, M., Pancost, R. D., Pearson, E. J., Peterse, F., Reichart, G.-J., Schaeffer, P., Schmitt, G., Schwark, L., Shah, S. R., Smith, R. W., Smittenberg, R. H., Summons, R. E., Takano, Y., Talbot, H. M., Taylor, K. W. R., Tarozo, R., Uchida, M., Dongen, B. E. van, Mooy, B. A. S. V., Wang, J., Warren, C., Weijers, J. W. H., Werne, J. P., Woltering, M., Xie, S., Yamamoto, M., Yang, H., Zhang, C. L., Zhang, Y., Zhao, M., and Damsté, J. S. S.: An interlaboratory study of TEX86 and BIT analysis of sediments, extracts, and standard mixtures, Geochemistry, Geophysics, Geosystems, 14, 5263–5285, https://doi.org/10.1002/2013GC004904, 2013.

Schrag, D. P., Hampt, G., and Murray, D. W.: Pore Fluid Constraints on the Temperature and Oxygen Isotopic Composition of the Glacial Ocean, Science, 272, 1930–1932, https://doi.org/10.1126/science.272.5270.1930, 1996.

Sinninghe Damsté, J. S., Rijpstra, W. I. C., Hopmans, E. C., Weijers, J. W. H., Foesel, B. U., Overmann, J., and Dedysh, S. N.: 13,16-Dimethyl Octacosanedioic Acid (iso-Diabolic Acid), a Common Membrane-Spanning Lipid of Acidobacteria Subdivisions 1 and 3, Applied and Environmental Microbiology, 77, 4147–4154, https://doi.org/10.1128/AEM.00466-11, 2011.

Smoliński, S., Denechaud, C., Leesen, G. von, Geffen, A. J., Grønkjær, P., Godiksen, J. A., and Campana, S. E.: Differences in metabolic rate between two Atlantic cod (*Gadus morhua*) populations estimated with carbon isotopic composition in otoliths, PLOS ONE, 16, e0248711, https://doi.org/10.1371/journal.pone.0248711, 2021.

Solomon, C. T., Weber, P. K., Joseph J Cech, J., Ingram, B. L., Conrad, M. E., Machavaram, M. V., Pogodina, A. R., and Franklin, R. L.: Experimental determination of the sources of otolith carbon and associated isotopic fractionation, Canadian Journal of Fisheries and Aquatic Sciences, 63, 79–89, https://doi.org/10.1139/f05-200, 2006.

Spezzaferri, S.: Planktonic foraminiferal paleoclimatic implications across the Oligocene-Miocene transition in the oceanic record (Atlantic, Indian and South Pacific), Palaeogeography, Palaeoclimatology, Palaeoecology, 114, 43–74, https://doi.org/10.1016/0031-0182(95)00076-X, 1995.

Spötl, C. and Vennemann, T. W.: Continuous-flow isotope ratio mass spectrometric analysis of carbonate minerals, Rapid Communications in Mass Spectrometry, 17, 1004–1006, https://doi.org/10.1002/rcm.1010, 2003.

Tierney, J. E. and Tingley, M. P.: BAYSPLINE: A New Calibration for the Alkenone Paleothermometer, Paleoceanography and Paleoclimatology, 33, 281–301, https://doi.org/10.1002/2017PA003201, 2018.

Titschack, J., Joseph, N., Fietzke, J., Freiwald, A., and Bromley, R. G.: Record of a tectonically-controlled regression captured by changes in carbonate skeletal associations on a structured island shelf (mid-Pleistocene, Rhodes, Greece), Sedimentary Geology, 283, 15–33, https://doi.org/10.1016/j.sedgeo.2012.11.001, 2013.

Trueman, C. N., Chung, M.-T., and Shores, D.: Ecogeochemistry potential in deep time biodiversity illustrated using a modern deep-water case study, Philosophical Transactions of the Royal Society B: Biological Sciences, 371, 20150223, https://doi.org/10.1098/rstb.2015.0223, 2016.

Trueman, C. N., Artetxe-Arrate, I., Kerr, L. A., Meijers, A. J. S., Rooker, J. R., Sivankutty, R., Arrizabalaga, H., Belmonte, A., Deguara, S., Goñi, N., Rodriguez-Marin, E., Dettman, D. L., Santos, M. N., Karakulak, F. S., Tinti, F., Tsukahara, Y., and Fraile, I.: Thermal sensitivity of field metabolic rate predicts differential futures for bluefin tuna juveniles across the Atlantic Ocean, Nat Commun, 14, 7379, https://doi.org/10.1038/s41467-023-41930-2, 2023.

Van Hinsbergen, D. J. J., Krijgsman, W., Langereis, C. G., Cornée, J.-J., Duermeijer, C. E., and Van Vugt, N.: Discrete plio-Pleistocene phases of tilting and counterclockwise rotation in the southeastern Aegean arc (Rhodos, Greece): Early Pliocene formation of the south Aegean left-lateral strike-slip system, J. Geol. Soc., 164, 1133–1144, https://doi.org/10.1144/0016-76492006-061, 2007.

Vasiliev, I., Karakitsios, V., Bouloubassi, I., Agiadi, K., Kontakiotis, G., Antonarakou, A., Triantaphyllou, M., Gogou, A., Kafousia, N., Rafélis, M. de, Zarkogiannis, S., Kaczmar, F., Parinos, C., and Pasadakis, N.: Large Sea Surface Temperature, Salinity, and Productivity-Preservation Changes Preceding the Onset of the Messinian Salinity Crisis in the Eastern Mediterranean Sea, Paleoceanography and Paleoclimatology, 34, 182–202, https://doi.org/10.1029/2018PA003438, 2019.

Wang, P., Tian, J., and Lourens, L. J.: Obscuring of long eccentricity cyclicity in Pleistocene oceanic carbon isotope records, Earth and Planetary Science Letters, 290, 319–330, https://doi.org/10.1016/j.epsl.2009.12.028, 2010.

Weijers, J. W. H., Schouten, S., Hopmans, E. C., Geenevasen, J. A. J., David, O. R. P., Coleman, J. M., Pancost, R. D., and Damsté, J. S. S.: Membrane lipids of mesophilic anaerobic bacteria thriving in peats have typical archaeal traits, Environmental Microbiology, 8, 648–657, https://doi.org/10.1111/j.1462-2920.2005.00941.x, 2006.

Wurster, C. M. and Patterson, W. P.: Metabolic rate of late Holocene freshwater fish: evidence from δ13C values of otoliths, Paleobiology, 29, 492–505, https://doi.org/10.1666/0094-8373(2003)029<0492:MROLHF>2.0.CO;2, 2003.

Zelck, C. and Klein, B.: Distribution of the lanternfish *Ceratoscopelus maderensis* (Lowe 1839) off Northwest Africa and its relation to water mass, Deep Sea Research Part I: Oceanographic Research Papers, 42, 1411–1422, https://doi.org/10.1016/0967-0637(95)00062-B, 1995.

van der Zwaan, G. J., Jorissen, F. J., and de Stigter, H. C.: The depth dependency of planktonic/benthic foraminiferal ratios: Constraints and applications, Marine Geology, 95, 1–16, https://doi.org/10.1016/0025-3227(90)90016-D, 1990.